INTERNAL DOCUMENT 263

I.O.S.

Development of a new low drag cable-fairing for the IOS SeaSoar system

by

A R Packwood

Internal Document No 263

August 1986

NATURAL ENVIRONMENT RESEARCH COUNCIL

INSTITUTE OF OCEANOGRAPHIC SCIENCES

INSTITUTE OF OCEANOGRAPHIC SCIENCES

Wormley, Godalming,
Surrey GU8 5UB
(042-879-4141)

(Director: Dr. A. S. Laughton, FRS)

Bidston Observatory,
Birkenhead,
Merseyside L43 7RA
(051-653-8633)
(Assistant Director: Dr. D. E. Cartwright, FRS)

Development of a new low drag cable-fairing for the IOS SeaSoar system

by

A R Packwood

Internal Document No 263

August 1986

Institute of Oceanographic Sciences
Brook Road
Wormley
GODALMING
Surrey
GU8 5UB

Contents

Development of a new low drag cable-fairing for the IOS SEASOAR system

1. Introduction

The SEASOAR system is used to measure a variety of parameters in the upper layers of the ocean. It is routinely used to measure conductivity and temperature against depth along a ships track. The system comprises a towed vehicle which has horizontal planes capable of generating both lift and down-force, some 600 m of multi-core conducting cable and a large vertical axis winch plus hydraulic power pack and deck-unit electronics for control and data handling. The sensor package in the body is towed on the conducting cable behind a ship and the planes on the vehicle are driven to make it undulate from near surface to between 200 - 400 m depth. The depth achieved depends upon ship speed, wire out, maximum wing down angle, the drag of the vehicle and the drag of the cable. At ship speeds in excess of 3 - 4 kn it is the latter that restricts the vehicle to the shallower depths. To overcome this the cable is faired using an enclosed segmented fairing which wraps around the 8mm diameter cable. This proprietry fairing, known as Fathom Flexnose 478 series, is described in fig. 1. The best operating speed has been found by experience to be 8 kn. At this speed a maximum depth of 350 - 375 m can be achieved without overstraining the cable.

It has long been recognised that if the system could be operated at the typical ship passage speed of 10 kn and the vehicle made to dive deeper then this would greatly increase the possible utilization and usefulness of the sampling system as an oceanographic tool. Improvements could be made to the vehicle design but the performance of the cable and fairing overshadow any hydrodynamic improvements that could be made in that area. If the cable-fairing drag could be substantially reduced then the increases in ship speed and vehicle depth desired could be achieved without greatly increasing the tension in the cable and possibly even reducing it.

In the following sections the performance of the present Fathom fairing is reviewed. The developments of a new fairing from early wind-tunnel trials of simple shapes, to numerical modelling and predictions of an efficient section shape are described. This is followed by tunnel testing of the chosen design. Finally practical design considerations of materials, fabrication and assembly are outlined.

2. Performance of the existing Fathom fairing

The School of Engineering at the University of Bath have undertaken a number of studies into the efficiency and behaviour of the proprietry Fathom fairing. The fairing they investigated was for a 16mm diameter cable and had a chord length of 80mm but was of a similar section shape to that shown in fig. 1. The Bath University tests were conducted at a Reynolds number based on the fairing chord of approximately 2.2×10^5, which corresponded to a ship speed of 6 kn.

Henderson (1978) reports the wind-tunnel tests of the larger fairing and the results are shown in fig. 2. The minimum C_D was 0.04 and the equivalent 2D lift-curve slope was 4.06. Most significantly the position of the aerodynamic centre (x_{ac}) was at only 15.4% chord. The aero-centre position is given by the slope of the $C_{MLE} \sim C_L$ curve

$$x_{ac} = - \frac{dC_{MLE}}{dC_L}$$

Note that the C_M values of fig. 2 are taken about the wire centre at x = 0.125 and not about the leading edge (x = 0).

The distance of the aero-centre aft of the wire centre at a given lift is directly proportional to the restoring moment that tends to make the fairing trail correctly and remain aligned with the flow. If it does not trail correctly then the drag is increased and a lift or side force develops which will tend to bring the towed vehicle up toward the surface. Wingham (1984) discusses this problem and comments that misalignments of as little as 0.1° can generate unacceptably high lifting forces where considerable lengths of faired cable are employed. The poor (x_{ac}-x_w) value for the Fathom fairing was due to the poor pressure distribution which peaked close to the leading edge subjecting much of the boundary layer to an adverse pressure gradient. This caused the laminar boundary layer to separate forming a laminar separation bubble, as observed by Henderson (1978), close to the maximum thickness point. In turn this led to the early turbulent separation which Henderson observed at ~ 85% chord.

Wingham and Keshavan (1978) reckon the minimum C_D measured by Henderson to represent the best or clean C_D for the fairing and estimate that this could rise to 0.055 through a variety of manufacturing and rigging imperfections. Note that values of C_D quoted in Wingham and Keshavan (1978) are based on thickness and not chord. In this paper C_D based on chord will be used throughout unless otherwise stated.

Furthermore Wingham (1984) highlights the importance of the weight of the fairing in water. If the fairing is "heavy" then when inclined and trailing in the water it may tend to flop to one side generating a small angle of incidence which in turn can lead to lift/side force and poor performance. The Fathom fairing is slightly heavy in water, approximately 1 N/m for the 80mm chord version.

The present fairing is stacked on the cable in 2 m lengths i.e. ~ 20 individual sections, supported at the bottom of each length by a stopper that is mechanically fitted or bonded to the cable. A short gap of 5 - 10 cm is then left between lengths. This method of attachment means that stacking loads induced by the weight of the fairing and, more importantly, hydrodynamic loads tangential to the cable build up along each length. The stacking load increases friction between neighbouring segments which can prevent correct alignment with the flow. Henderson (1978) discusses this in some detail and indicates the lengths they had to go to in order to reduce the friction.

An alternative method of attaching the lengths of fairing to the cable would be to suspend it from the top of each length. This would reduce the stacking load to zero but would create small gaps between neighbouring segments. Wingham and Keshavan (1978) observed a 2mm gap to increase C_D by ~ .005. However this drag increase is at least as large as that measured by the same authors for the effects of "fantailing" and "sawtoothing" which can be engendered by the stacking loads. It was decided therefore to investigate the alternative suspension method and the effects of the multiple small gaps ($\leqslant$ 2mm).

In summary it was apparent that there were several areas where improvements could be made.

1) reduce the drag by delaying transition and preventing early turbulent separation.

2) move the aero-centre aft by modifying the pressure distribution thus increasing the stabilizing restoring moment.

3) make the fairing lighter or buoyant to reduce flopping.

4) modify the suspension method to reduce stacking loads to zero.

3. Initial trial-section shapes

Early attempts to find a good section shape were empirical. A NACA 0021 aerofoil shape was selected as a starting point. The NACA 0021 was chosen from Abbott and von Doenhoff (1959) for its generally good characteristics and suitable thickness distribution. A 2D wooden model at twice proposed full scale of 1 m span and 120mm chord was constructed and tested in Bath University wind-tunnel at Re = 3.1×10^5. This is roughly equivalent to 14 kn ship speed, which is the maximum ship speed for IOS research vessels. The final design Re for approx 10 kn ship speed would probably be between 2 and 2.5×10^5 - dependent on the chosen chord length. The section shape is shown in fig. 3 and the results in fig. 4. Principle results are summarized in table 1. A lower drag coefficient was achieved but the distance between the location of the wire centre and aero-centre was only 6.3% chord.

To try and improve this the nose was heavily rounded to put the wire centre as far forward as possible, see fig. 3. This modification, designated water-foil 1 or WF1 with c = 110mm, was likewise tested but at the slightly reduced Re of 2.8×10^5. Again results are shown in fig. 4 and table 1. The minimum drag was increased to 0.032, the lift-curve slope dropped by 18% and the aero-centre moved forward to 19% chord. The separation between wire and aero-centre increased to 9%. The results also showed an early stall at -6° and separation bubbles were observed at 0° together with separation ~ 10% ahead of the trailing edge.

It was concluded that the improvement in aero-centre moment arm was not worth the drag penalty. Clearly at these relatively low Reynolds numbers (normal aerofoils rarely operate below Reynolds numbers of 2 million) something more subtle had to be done to achieve low-drag attached flow for a reasonably sized aerofoil with good wire-centre to aero-centre separation. It would be possible to just scale up the NACA 0021 to achieve a good wire-aero centre separation but this would present greater storage problems on the winch and

increase the overall drag.

In the search for a low drag "thick" strut other researchers have developed some very extreme though highly efficient shapes. Williams (1977) designed a 40% thick, round nosed fairing which operated well at Re = 1.5×10^6 but the performance significantly deteriorated for Re < 10^6 due to flow separation. Smith (1972) shows a 46% thick tear-drop shape for operating at Re = 5×10^6 and Calkins (1982) examines a similar section designed by Liebeck as a potential design for a cable-fairing. Although such fairings can achieve very low drag coefficients, their behaviour is very Reynolds number dependent and the aero-centre can be as far forward as 5% chord. Calkins discovered that the stability of the Liebeck section could be improved by the addition of trailing edge wedges. These however increased drag and would be easily damaged in shipboard handling. What is required for routine shipbourne use is a less extreme shape, less dependent on Reynolds number, with good weather-vane stability about the rotation centre, i.e. the wire centre.

4. Theoretical development of the new optimized section

From the earlier tests several things were clear. The highly rounded nose of the Fathom and WF1 sections caused the pressure distribution to peak near the leading edge. Consequently much of the boundary layer was subject to an adverse pressure gradient. This, together with the fact that Re was relatively low, was the cause of the flow separation ahead of the trailing edge, the consequent high drag and forward shifted aero-centre which would normally reside at about the quarter chord for a section with attached flow.

At this point advice was sought from the Aerodynamics Department at the Royal Aircraft Establishment, Farnborough. They quickly agreed that control of the boundary layer was crucial in the Re range 2×10^5 < Re < 3×10^5. To assist the research project RAE agreed to pass to IOS a much simplified version of their 2D wing section analysis program. The full method is described in some detail in Williams (1985). The simplified version performs an inviscid calculation to determine the force and moment coefficients and pressure distribution for the aerofoil at any given incidence. The program then uses the pressure and velocity distributions to estimate the boundary layer characteristics including transition, laminar separation and reattachment and

turbulent separation points. This represents only the first iteration of the full method which goes on to recalculate the equivalent inviscid flow and boundary layer characteristics until successive iterations show the solution to have converged.

The purpose of using the simplified version as opposed to the full viscous analysis program in these initial stages was because the simplified version was relatively quick and cheap to run while still providing a guide to the boundary layer behaviour. This proved to be of advantage as the analysis program can only be used in a cut and try manner. Hence many shapes could be investigated quickly and cheaply. Figures 5-7 show results from the simplified program for the three sections discussed so far, i.e. Fathom fairing, NACA 0021 and WF1, all at a Reynolds number of 2.5×10^5. At this Reynolds number all, under conditions of natural transition, exhibited a laminar separation bubble. Comparing these solutions clearly demonstrated that delaying transition was important in achieving low drag.

The values of C_D given in figs 5-7 were calculated using Squire and Young's formula which was applied in the wake region. This gives

$$C_D = 2\theta U^{0.5(H+5)}$$

where θ, U and H are predicted by the analysis program. Significantly the drag figures calculated in this way were all lower than the measured values, given in table 1, by factors ranging from 2 → 3. However the trend emerging from the progression of section shapes was similar.

A series of numerical trials were conducted using the simplified analysis program varying the section shape and Reynolds number. It became clear that it would be possible to maintain a laminar boundary layer back to approximately 50% chord provided the pressure distribution did not come to a sharp peak, but rose gradually to approximately $C_p = -0.8$. To keep the turbulent boundary layer attached a Stratford-type pressure recovery was required. The feature of the Stratford pressure rise is that the initial rate of pressure recovery is high and then reduces toward the trailing edge. This form of pressure recovery keeps the turbulent boundary at the point of incipient separation and therefore the skin friction is very low. Smith (1972) gives a detail description of the Stratford pressure rise.

A design Reynolds number of 2.5×10^5 was eventually settled upon. The higher the Reynolds number the easier the boundary layer would be to control but increasing the chord length implies increased skin friction drag tangential to the cable axis and hence higher cable tensions. Therefore some compromise was necessary. For a design ship speed of 10 kn the chosen Re gave a fairing chord length of 70mm. This was 20mm longer than the Fathom fairing.

To speed the cut and try iteration process RAE decided to employ a design method to predict the aerofoil shape given a desired form for the pressure distribution. The method is described in Fiddes and Hogan (1986). First the method examines a family of pressure distributions, similar to the desired form, allowing the trailing edge pressure to vary and then optimizing the drag and lift/drag characteristics. Secondly it uses an inverse inviscid method to determine the thickness distribution for the section using the optimized pressure distribution.

The form of the design C_p distribution was specified as having a roof-top pressure distribution with a suction peak of $C_p > -0.8$ back to 55% chord followed by a rapid pressure recovery. Two shapes, WF2 and WF5, generated using the design program, are shown in figs 8 and 9. Section WF2 has a steeper gradient to the suction peak and hence a more rounded nose than section WF5. Both of these sections were run through the full viscous aerofoil analysis program, allowing free transition, giving the results summarized in table 2. Both sections featured a laminar separation bubble of length 15% centred at 48% chord in the case of WF2 and 49% in WF5. However according to the Granville stability correlation, which is used in the analysis program, WF5 had the more stable laminar boundary layer. The position at which initial instability was predicted (xi) was 3% further aft for WF5. Despite the fact that with the more rounded nose the wire centre could be shifted 1.5% further forward in WF2, it was decided that WF5 was the preferred section because of its lower suction peak and more stable boundary layer.

The appearance of a separation bubble at these low Reynolds numbers was not surprising. The requirement for the leading edge to be well rounded in order that the wire centre may be kept well forward was not conducive to suppressing bubble formation. The analysis program uses Horton's method (see Horton (1967)) to calculate the length of the bubble. Very approximately the non-dimensional bubble length lies in the range

$(4 \rightarrow 6) \times 10^4/Re$

i.e. reducing Re has the effect of increasing the length of the bubble. Long bubbles are more prone to bursting i.e. failing to reattach, and so should be avoided. It could be expected therefore that the section would perform less well at lower Reynolds numbers. However from the predictions shown in table 2 the bubble did not appear to seriously adversely influence the drag or position of the aero-centre.

A practical change, proposed for ease of handling, manufacture and because of the likelihood of damage in service, was to cut off the sharp trailing edge. This was done by scaling up the section and cutting off the end so that the chord length of 70 mm was retained but the trailing edge was approx 2mm thick at full scale. This section with the thick trailing edge was designated WF5T.

Table 3 shows the results obtained on running both the simplified and the full viscous analysis programs for the modified geometry WF5T with natural transition. For the simplified model it should be remembered that C_L and C_M are given by the inviscid calculation and C_D was calculated by applying Squire and Young's formula in the wake region. Comparing the results from the simplified and full viscous analysis programs showed that the boundary layer behaviour and the drag were in good agreement. Where the simplified model fell down was in the calculation of the lift and pitching moment, which it overestimated by 20 - 30% in this case. The drag of WF5T was little changed compared with WF5, but the separation bubble, still in evidence, was shifted back approximately 5%. It was thought that the bubble might be suppressed by tripping the boundary layer and forcing transition just ahead of the natural laminar separation point. From table 3 the obvious location for the trip at $Re = 2.5 \times 10^5$ was at 50% chord. In practise it was throught that this might be achieved by moving the join between nose and tail pieces, marked (A) in fig. 1, back to half chord.

Section WF5T with transition fixed on upper and lower surfaces at $x = 0.5$ was consequently analysed using the full viscous program.

Fig. 10 (a - e) plots the calculated pressure distributions for a range of incidences at $Re = 2.5 \times 10^5$. Primary results are summarized in table 4, which also shows results for the lower Reynolds numbers of 2×10^5 and 1.5×10^5. $C_L \sim \alpha$, $C_D \sim C_L$ and $C_{MLE} \sim C_L$ curves are also plotted in fig. 11 (a - c).

The plotted pressure distributions show how the full viscous solution diverged from the inviscid solution, the differences becoming more apparent with increasing incidence as the viscous lift decreased due to the thickening boundary layer. The program predicted the forward migration of the laminar separation bubble on the upper surface as shown in fig. 10 (a - e). The analysis further predicted that the section was likely to stall at an incidence between 6 → 7° with $C_{LMAX} \sim 0.55$. In lift and pitching moment there were only slight variations with Reynolds number, the lift curve slope being ~ 6.1 and $x_{ac} \simeq 0.25$. The minimum drag (C_{DO}) at the design Reynolds number was calculated to be 0.012. Fig. 11b shows a substantial rise in drag with decreasing Reynolds number, C_{DO} was increased by 50% at the lowest Re. At Re = 1.5×10^5, and $\alpha = 1°$ the method failed to converge suggesting it found difficulty in reattaching the separation bubble, however this was not the case for the other incidences investigated. This might suggest that the separation bubble was close to bursting at this low Reynolds number.

The low drag, between 25% and 50% of the measured Fathom fairing drag, and the favourable aero-centre location made section WF5T an attractive design in terms of its potential performance. It should be remembered that these numerical predictions were strictly two dimensional. No allowance was made for the aspect ratio of individual sections or for the gaps between them. It was decided however that WF5T was a viable design worthy of wind-tunnel investigation.

5. Wind-tunnel tests on section WF5T

The trials were carried out in the 3ft x 4ft low turbulence RAE wind-tunnel. Two wooden models of section twice full scale and 40in span were constructed. The first was of constant section across the span, 2D, and would be used to make comparisons with the results obtained using the numerical models. The second had 4mm gaps at 200mm intervals to be more representative of the final assembled 3D fairing. Both had a knife cut at 50% chord on upper and lower surfaces running full span to represent the joint between nose and tail pieces. Both were fitted with end plates and painted matt black. Fig. 12 shows the 3D model mounted in the tunnel. Measurements of lift, drag and pitching moment at Re = 2.5×10^5 were made on both models. The 3D model was also run at Re = 2×10^5 and 1.5×10^5. In all tests an incidence range of -4° to +10° was

investigated. The 2D model was run with end plates on and off, so that the end plate drag could be evaluated. All of the wind-tunnel corrections are shown in the Appendix. Wind-off tare measurements were taken before and after each run.

5.1 2D tests

Fig. 11 (a - c) plots the C_L, C_D and C_{MLE} results for the 2D fairing model tested between end plates at Re = 2.5 x 10^5 which, for the 140mm chord model, was a wind speed of 26 m/s. These are superimposed on the earlier curves predicted by the full viscous analysis program. Several things are worthy of note, the lift-curve slope and the slope of the pitching moment curve were fairly close to that predicted, but the predicted stall was not evident in the range investigated. Fig. 11b shows that the measured drag was much higher than predicted, approximately 0.02 at C_L = 0 compared with 0.012.

Flow visualization tests were carried out using flourescein-sodium dye in paraffin photographed using ultra-violet flash photography. The mixture was applied to the model surface using a sponge and the tunnel was then run until the flow patterns had developed. The results for the 2D model tests are shown in fig. 13. Comparison of the flow separation and reattachment lines indicated in fig. 13 with the numerical predictions of table 4 and fig. 10 indicate that laminar separation occurred earlier and the bubble length was longer than predicted. This may be the reason for the discrepancy in drag. No trailing edge separation was apparent from the flow visualization and this was borne out by the pitching moment curve (fig. 11c) which gave the aero-centre to be at x_{ac} = 0.248 suggesting that the flow was attached.

5.2 3D tests

The results obtained from testing the second model between end plates with 4mm gaps at 200mm spacing, are shown in figs. 14, 15 and 16. Fig. 14 (a - c) plots the force and moment coefficients while figs 15 (a - i) and 16 (a - e) show the flow visualization results. Tests were conducted at three Reynolds numbers, 2.5 x 10^5, 2.0 x 10^5 and 1.5 x 10^5. To back up the oil-flow tests, which at low Reynolds number can be difficult to interpret, a china-clay technique was also employed. Details of the technique are described in Moir (1984). Fine china-clay in a laquer was sprayed onto the model surface, when this had dried, a volatile indicator, in this case oil of winter-green, was sprayed on and the

tunnel run up to speed until the preferential drying patterns had emerged. The white areas in figs 15 (b,c,e,f,h,i) show up areas of high skin friction i.e. under a laminar boundary layer near the leading edge where the shear is high or under a turbulent boundary layer. Care needs to be taken in interpreting these pictures for dark or clear areas may not always indicate separated flow, but just areas where the skin friction was very low i.e. in the turbulent boundary layer under the Stratford pressure rise. A small lump of plasticine was stuck to the underside of the fairing near the leading edge, seen to the left on fig. 15b, to indicate the optimum time at which to stop the tunnel.

The lift-curve slope at Re = 2.5 x 10^5 was slightly less than in the 2D case as might be expected. Remarkably however the minimum drag was only fractionally higher and the position of the aero-centre, as given by the slope of the pitching moment curve, was little changed. This was very encouraging. The flow visualization at α = 0° (fig. 15a, b, c) indicated the presence of a long laminar separation bubble between ~ 30 - 70% chord. As the incidence was increased the bubble moved forward on the suction surface and back on the pressure surface in general agreement with the numerical model. However, the bubble was significantly longer than predicted. The line cut on the surface at 50% chord appeared to have little influence on fixing transition or preventing bubble formation. From fig. 15f it may be deduced that a bubble existed between 50 - 75% on the pressure surface which would be roughly in line with the natural transition predictions shown in Table 3. As with the two dimensional section, there was no evidence of stall up to 10°. Fig. 15h may indicate some separated flow on the suction surface at α = 8°, just a few percent ahead of the trailing edge, but this is debatable.

Fig. 17 shows the drag coefficient plotted against C_L^2 for both models at the design Reynolds number. It revealed that the 3D fairing had apparently 45% more induced drag than the 2D fairing. Induced drag or lift dependant vortex drag is proportional to C_L^2 and inversely proportional to aspect ratio. The gaps reduce the effective aspect ratio and introduce discontinuities from which vortices are shed. The behaviour is roughly consistent with other observations of wings with gaps reported in Hoerner (1965).

5.3 Tests at lower Reynolds numbers

Results for the runs at the lower Reynolds numbers are superimposed on fig. 14 and the flow visualization results are shown in fig. 16. The lift-curve slope dropped 12% on decreasing Re to 2×10^5 and a further 2% when Re was reduced to 1.5×10^5. The largest notable change was in C_{D0} which increased from .021 at Re = 2.5×10^5 to .032 at Re = 1.5×10^5. Otherwise the shape of the $C_D \sim C_L$ curves were similar. For all the Re's investigated the aero-centre shifted very little, but hovered around the quarter chord point.

Consistent with theoretical predictions the laminar bubble appeared to grow in extent with decreasing Re. It occupied 30 → 65% chord at Re = 2×10^5 and approximately 25 → 75% at Re = 1.5×10^5, although in the latter case the location of the laminar separation (x_ℓ) appeared to vary considerably from upper to lower surface (see fig. 16d - e). Again the cut at x = 0.5 appeared to have little influence and the flow patterns appeared to follow the trends predicted numerically for natural transition. There was no evidence from the force and moment measurements or the flow visualization to suggest that the laminar bubble had burst within the incidence or Reynolds number ranges investigated.

5.4 Conclusions drawn from the wind-tunnel tests

Two significant differences were found between the numerical predictions and the measurements:

i) The drag was significantly higher than predicted. The reason for this appeared to be that the laminar separation bubble was longer and separated slightly ahead of the point predicted.

ii) No fairing stall was evident up to the 10° maximum incidence investigated. This was conceivably due again to the longer separation bubble which meant that the turbulent boundary layer had less far to run to the trailing edge and therefore was not so prone to separation.

The theory applied in the analysis program only strictly applies to flows with short laminar separation bubbles and hence may be expected to be less reliable in low Reynolds number flows. In this respect the comparison shows that the method could be improved by including an interactive bubble

calculation. The present theory would better predict transition fixed performance but the cut line on the wind-tunnel model did not succeed in fixing transition.

The experiments show the true low Re behaviour for the section, i.e. higher drag but delayed stall. Comparing the results with the theoretical predictions suggests that if transition were fixed then drag at low incidence may be reduced but the section would stall earlier. This would be unacceptable. The analysis has successfully pointed out a good section shape but clearly wind-tunnel tests were necessary to give the true low Reynolds number performance.

A summary of all the wind-tunnel results discussed is shown in table 1. The force and moment measurements are also shown, superimposed for direct comparison, in fig. 18 (a - c). From these it can be seen that the fairing WF5T with the gaps had approximately half the drag of the existing Fathom section and the important wire centre to aero-centre separation was increased by a factor of 5. Also WF5T did not exhibit the early stall at ~ 4° incidence found by other authors in the case of the Fathom fairing. Clearly the WF5T section had the best overall performance, in terms of drag and aero-centre position, of all the other sections investigated.

The effect of the gaps on the drag was smaller than had been anticipated from scaling the results of Wingham and Keshaven (1978). They predicted a C_{DD} increase of 0.005 compared to the measured increase of 0.001. Since the WF5T section offered the significant improvements in performance that were looked for, it was chosen to go forward to the engineering design phase.

6. Engineering design considerations

6.1 Specification

i) In order that fairing sections may be easily replaced if damaged they must be capable of being assembled onto the cable without having to thread them onto the cable end. Hence individual sections must be capable of opening and closing neatly around the cable. It would be an advantage if this could be done without the use of tools or adhesives.

ii) The tail end of the fairing must be slightly buoyant to overcome the flopping tendency remarked upon in (2). Also the overall weight or buoyancy of the fairing in sea-water should be small compared with the weight of the wire, which is ~ 2 N/m in sea-water.

iii) The fairing should be suspended on the cable as suggested in (2) to reduce stacking loads to zero.

iv) The fairing must freely pivot on the wire so that it may align accurately with the flow. Therefore friction at the suspension points and between fairing and wire should be kept low.

v) The fairing and wire must be capable of passing over a sheave of minimum diameter 620 mm while under load (maximum load ~ 20 kN) at typical hauling/veering speeds of 1 m/s.

vi) The fairing should very closely conform to the section shape derived in this report with a good quality, smooth surface finish and no surface imperfections.

vii) The join between nose and tail pieces, should the fairing be made in two or more sections, should be at 50% chord.

viii) The materials used should not be degraded by sea-water, sunlight, hydraulic/lubricating oils or greases, and furthermore should be resilient and tough to withstand harsh treatment. They should also be able to withstand without significant deformation, hydrostatic pressures equivalent to at least 600 m of water.

ix) The gaps between the suspended fairing elements when under normal towing conditions should not, on average, exceed 2 mm.

6.2 Loads on the fairing while towing

The fairing is to be suspended on the cable in lengths made up of multiple segments joined by links. The drag component normal to the cable axis is low and is little changed from segment to segment. However the tangential drag

component is cumulative and is transferred to the cable at the suspension point at the top of each length. Following Eames (1968) the tangential drag is given by

$$P = \mu R \cos\phi$$

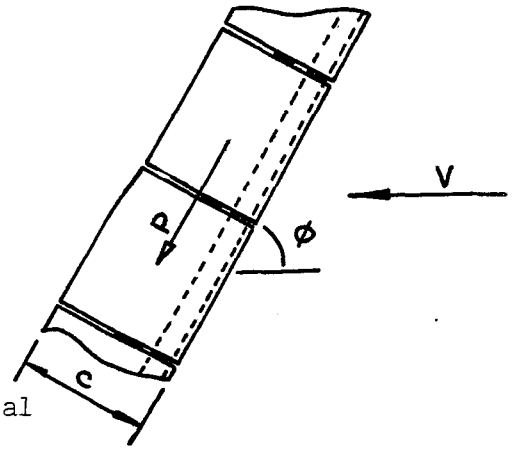

where $R = \frac{1}{2}\rho V^2 \, c \, C_{DO}$

C_{DO} is the normal drag coefficient based on chord

μ is the "friction ratio"

and ϕ is the angle of the cable to the horizontal

For a good enclosed fairing Eames suggests $\mu = 0.8$ to be appropriate. For fairing WF5T at 10 kn (5.144 m/s) $P \simeq 16 \cos \phi$ (N/m). If lengths of fairing were say 3 m long then the maximum load on the suspension point would be approximately 50 N. This would also be the maximum load in the topmost link.

The suspension mechanism will be a modified 6 mm aluminium alloy Talurit ferrule developed and tested at IOS. This will be compressed onto the cable using a hydraulic press tool. This fitting has been tested and will take loads of up to 1300 N without slipping. The fairing segment at the top of each link will have a cut-out in the leading edge enabling it to fit over the ferrule. One or two teflon coated split washers will be employed to act as a low friction bearing between the ferrule and where it bears on the fairing segment.

6.3 Requirements for passing over a sheave

The wire under a maximum load of order 2 tonnes will put great pressure on the fairing nose to conform to the diameter of the sheave wheel. For the 620 mm diameter wheel presently used a maximum segment length or span of 100 mm looks suitable. Even so the nose at the ends of each segment will need to stretch ~ 4 mm. Clearly a material with high elasticity will have to be used and the design must allow for this movement. Similarly the joining link will have to be elastic for this must stretch 7 mm. A compromise between the need to stretch easily when passing over a sheave and for the link not to stretch more than 2 mm under hydrodynamic loading has to be achieved.

6.4 Material selection

As has already been made apparent in (6.3) the nose and link must be of a highly elastic material. The nose must also be tough and abrasion resistant for passing over sheaves and winches. Polyurethanes with a Shore hardness of 80A → 95A and elongations of 400 → 600% at break would fit the requirement if the modulus of elasticity is matched to the loading and extension requirements. Polyurethane has a specific gravity of 1.07 and therefore could not be incorporated into the tail which has to be buoyant. For the tail a variety of materials appear suitable, polypropylene, with an s.g. of 0.9, if UV protected would suffice, or a foamed polypropylene or plastic alloy, e.g. Noryl, which can achieve even lower specific gravities would equally do, provided the foaming did not collapse under hydrostatic pressures.

All of these materials can be injection moulded, however tooling costs for injection moulding are high and an envisaged future demand for at least 20,000 units is necessary in order to offset the high mould costs. A run of 6000 would be sufficient to cover 600 m of cable. Injection moulding does offer advantages in terms of good surface finish, quality control and quick production once tooled up. Hence this is the method envisaged for production.

The proposed arrangement that it is hoped will fulfil the requirements and meet the specification is shown in fig. 19 (a - c). The fairing will thus comprise a flexible nose piece that will wrap around the cable, a relatively rigid plastic tail piece that will be buoyant and will slot onto the nose piece keeping it together and an elastic link made of the same material as the nose. The surface co-ordinates for the nose and tail sections conforming to the WF5T section are given in fig. 20.

7. Predicted overall system performance

Having arrived at a new design the important question remained of how much improvement on overall SEASOAR performance might be expected. To test this, numerical predictions of cable catenaries for the present Fathom fairing with a SEASOAR vehicle attached were compared with the proposed WF5T fairing. The numerical model is based on the hydrodynamic relations developed by Eames (1968) which calculates normal and tangential cable + fairing drag. The integration

scheme follows Mihoff (1966). A constant C_L was assumed for the winged vehicle developing a download of approximately 250 kgf at 8 kn. It should be noted that WF5T is slightly thicker and has a longer chord than the Fathom 478 series fairing. Normal drag coefficients for WF5T, based on thickness, of 0.1 at 10 kn and 0.125 at 8 kn were selected. For the Fathom fairing two conditions were assumed, a best C_{Dt} of 0.16, following Henderson (1978), and a worst C_{Dt} of 0.22, after Wingham and Keshavan (1978). A value of Eames' friction ratio of $\mu = 0.8$, which reflects the scale of the tangential friction component, was assumed for both. The calculated catenaries at towing speeds of 8 kn and 10 kn are shown in fig. 21. Table 5 summarizes the performance and gives the very important cable tension estimate at the ship end of the cable.

The results indicate that at 8 kn there is little to choose between WF5T and the "best" Fathom fairing, but there is a 50m increase in depth when compared with the "worst" Fathom drag case. At 10 kn the "worst" Fathom case develops tensions that are unacceptably high. However WF5T improves on the "best" Fathom fairing giving tensions 16% lower with a 40m increase in depth. WF5T could make 10 kn towing a feasible option with no loss in depth performance. Since the Fathom fairing in service probably operates somewhere between the "worst" and "best" cases investigated, improvements in depth from using WF5T of approximately 60 m may be achieved with tensions approximately 25% lower than could be obtained using the Fathom system at 10 kn. Only full scale testing can validate these predictions.

8. Conclusions

A new fairing with drag coefficient approximately 45% less than the presently used fairing has been developed. The fairing is ~ 3 mm thicker and 20 mm longer than the Fathom fairing and develops much stronger correcting moments to align it with the flow. The new fairing gives predicted depth improvements for the SEASOAR system of 15%. The towing tension appears sufficiently reduced to permit towing at 10 kn at depths approaching 400 m with 600 m of faired cable.

Acknowledgements

The author would like to acknowledge the valuable contributions made to this project by the RAE, Farnborough. In particular Dr. B.R. Williams for his invaluable assistance with the viscous modelling plus his helpful advice and comments, also Mr. S.P. Fiddes for the use of his inverse method and to Mr. I.R.M. Moir for carrying out the china clay flow visualization tests. Thanks are also due to Mr. W.J.G. Trebble and the staff of the RAE wind-tunnel section for their help in rigging and testing the models and to Mr. Harold Plato of IOS for his painstaking efforts in producing the models.

References

Abbott I.H. and von Doenhoff A.E. (1959) Theory of wing sections.
pub. Dover, New York, pp. 693.

Calkins D.E. (1982) An experimental and analytical investigation of the two-dimensional aero/hydrodynamic characteristics of bluff symmetrical fairing sections.
A1AA-82-0961.

Eames M.C. (1968) Steady state theory of towing cables.
Qu. Trans. Roy. Inst. of Naval Architects 110: 185 - 206.

Fiddes S.P. and Hogan M.J. (1986) A low-speed aerofoil design method - description and application.
RAE unpublished.

Henderson J.F. (1978) Some towing problems with faired cables.
Ocean Engng 5(2): 105 - 125.

Hoerner S.F. (1965) Fluid dynamic drag.
pub. Hoerner Fluid Dynamics, P.O. Box 342, Brick Town, N.J., USA.

Horton H.P. (1967) A semi-empirical theory for the growth and bursting of laminar separation bubbles.
ARC C.P. No. 1073, pp. 37.

Mihoff C.M. (1966) Configuration of a cable towing a submerged body.
Naval Res. Est. Dartmouth, N.S., USA. Tech. Note Math/66/1.

Moir I.R.M. (1984) Recent experience in the RAE 5 metre wind tunnel of a china-clay method for indicating boundary layer transition.
RAE Tech. Memo. Aero 2007, pp. 10.

Smith A.M.O. (1972) Aerodynamics of high lift airfoil systems.
NATO - AGARD 10: 1 - 24

Williams B.R. (1977) Design and testing of a 40% thickness-to-chord ratio symmetrical fairing.
RAE TR 77168.

Williams B.R. (1985) The prediction of separated flow using a viscous-inviscid interaction method.
The Aeronautical Journal of the Royal Aeronautical Soc. May 1985, pp. 185 - 197.

Wingham P.J. (1984) Some causes and effects of tow off.
Ocean Engng 11(3): 281 - 313.

Wingham P.J. and Keshavan N.R. (1978) Predicting the equilibrium depth of a body towed by a faired cable.
Ocean Engng 5: 15 - 35.

Notation

C_D	drag coefficient = drag force/($\frac{1}{2}\rho V^2 S$)
C_{D0}	C_D at $\alpha = 0$
C_{Dt}	C_D based on thickness $C_{Dt} = C_D/t$
C_L	Lift coefficient = lift force/($\frac{1}{2}\rho V^2 S$)
C_M	pitching moment coefficient = pitching moment/($\frac{1}{2}\rho V^2 Sc$)
C_P	pressure coefficient = pressure/($\frac{1}{2}\rho V^2$)
c	chord length
H	boundary layer or wake shape factor
Re	Reynolds number = cV/ν
S	section plan area
t	non-dimensional section thickness = thickness/c
U	non-dimensional wake velocity = velocity/V
V	free stream fluid velocity
x	non-dimensional distance from leading edge = distance/c
α	angle of incidence of the section to the flow
Θ	non-dimensional momentum thickness in the wake = momentum thickness/c
μ	Eames' friction ratio = tangential friction/normal friction
ν	kinematic fluid viscosity
ρ	fluid density

- other symbols are explained in the text.

Further subscripts

ac	aero-dynamic centre
ep	end plates
LE	leading edge
tc	tunnel constraint
c/4	quarter chord point
i	initial boundary layer instability point
ℓ	laminar separation point
r	reattachment point
s	turbulent separation point
w	wire centre
p	pivot point

TABLE 1 Summary of wind-tunnel test results

SECTION	Re $\times 10^5$	c (mm)	x_w	C_{DO}	$\frac{dC_L}{d\alpha}$	x_{ac}	$x_{ac}-x_w$	t
FATHOM Henderson(1978)	2.08	80	.125	.040	4.06	.154	.029	.25
NACA 0021	3.1	120	.152	.019	4.63	.215	.063	.21
WF1	2.8	110	.10	.032	3.78	.190	.090	.227
WF5T 2D	2.5	140	.095	.020	5.72	.248	.153	.225
3D	2.5	140	.095	.021	5.34	.254	.159	.225
3D	2.0	140	.095	.028	4.69	.246	.151	.225
3D	1.5	140	.095	.032	4.58	.250	.155	.225

TABLE 2 Results predicted by the full viscous analysis for sections WF2 and WF5 at Re = 2.5 x 10^5

WF2: $x_w = .08$ $x_{ac} = .240$

$\alpha°$	C_L	C_D	C_{MLE}	upper surface x_i	upper surface $x_\ell - x_r$	upper surface x_s	lower surface x_i	lower surface $x_\ell - x_r$	lower surface x_s	Cp_{max}
0	0	.0122	0	.17	.45-.60	-	.17	.45-.60	-	-0.77
1	.1145	.0123	-.0285	.14	.43-.57	-	.21	.48-.64	-	-0.93
2	.2259	.0126	-.0558	.11	.38-.51	-	.24	.49-.65	-	-1.12
5	.5304	.0158	-.1277	.06	.21-.32	-	.37	.52-.69	-	-1.86

WF5: $x_w = .095$ $x_{ac} = .247$

0	0	.0119	0	.2	.46-.61	-	.2	.47-.63	-	-0.72
1	.1142	.0119	-.0289	.17	.44-.58	-	.23	.48-.64	-	-0.85
2	.2240	.0122	-.0562	.14	.39-.52	-	.27	.5 -.65	-	-1.0
5	.5385	.0146	-.1330	.09	.24-.36	-	.38	.53-.69	-	-1.58

x_i = initial boundary layer instability detected

x_ℓ = laminar separation point

x_r = reattachment point

x_s = turbulent separation point - if ahead of the trailing edge

TABLE 3 Computed results obtained using the RAE analysis programs for section WF5T with natural transition

Re = 2.5 x 10^5 full viscous analysis

$\alpha°$	C_L	C_D	C_{MLE}	upper surface				lower surface			
				x_i	x_ℓ	x_r	x_s	x_i	x_ℓ	x_r	x_s
0	-.0014	.0118	+.0006	.21	.52	.67	-	.21	.52	.67	-
1	.1101	.0119	-.0281	.18	.48	.63	-	.25	.54	.69	-
2	.2149	.0123	-.0539	.16	.43	.57	-	.28	.55	.71	-
3	.3152	.0129	-.0780	.14	.38	.51	-	.31	.56	.72	-
4	.4103	.0137	-.1001	.11	.33	.46	-	.36	.58	.74	-
5	.4978	.0147	-.1191	.10	.28	.40	-	.4	.58	.75	-

Re = 2.5 x 10^5 simplified analysis

								lower surface			
								x_i	x_ℓ	x_r	x_s
0	-.0001	.0110	0	.21	.51	.66	-	.21	.51	.66	-
1	.1287	.0109	-.0362	.18	.48	.62	.99	.25	.53	.69	-
2	.2575	.0120	-.0723	.15	.43	.56	.99	.29	.55	.70	-
5	.6431	.0142	-.1801	.09	.27	.39	.81	.42	.58	.75	-

TABLE 4 Computed results obtained using the RAE full viscous analysis program for section WF5T with the boundary layer tripped at x = 0.5

Re = 2.5 x 10^5

$\alpha°$	C_L	C_D	C_{MLE}	upper surface x_i	x_ℓ	x_r	x_s
0	.0270	.0120	-.0076	.20	.50	.65	-
2	.2404	.0125	-.0620	.15	.43	.56	-
4	.4201	.0143	-.1037	.11	.30	.43	-
5	.5012	.0155	-.1204	.10	.26	.38	-
6	.5502	.0171	-.1242	.08	.22	.34	.92
7	.3809	.0219	-.0570	.08	.21	.33	.70

Re = 2.0 x 10^5

0	.0309	.0155	-.0105
1	.1626	.0155	-.0465
2	.2675	.0158	-.0727
3	.3610	.0164	-.0942
4	.4444	.0174	-.1120
5	.5149	.0186	-.1241
6	.5343	.0200	-.1159

Re = 1.5 x 10^5

0	.0536	.0179	-.0204
1	bubble burst - flow fails to reattach		
2	.2851	.0187	-.0796
3	.3794	.0191	-.1015
4	.4313	.0207	-.1068
5	.5126	.0213	-.1230
6	.4957	.0235	-.1010

TABLE 5 **Comparison of system performance with 600m of faired cable**

Fathom 478 C_{Dt} = 0.16

Tow speed (kn)	Tension @ ship (kN)	Vehicle depth (m)	Vehicle trail (m)
8	10.5	384	433
10	15.8	352	457

Fathom 478 C_{Dt} = 0.22

Tow speed (kn)	Tension @ ship (kN)	Vehicle depth (m)	Vehicle trail (m)
8	13.4	331	472
10	20.5	300	491

WF5T

Tow speed (kn)	C_{Dt}	Tension @ ship (kN)	Vehicle depth (m)	Vehicle trail (m)
8	0.125	10.4	386	432
10	0.1	13.2	391	428

Fig. 1 Fathom Flexnose 478 series fairing section

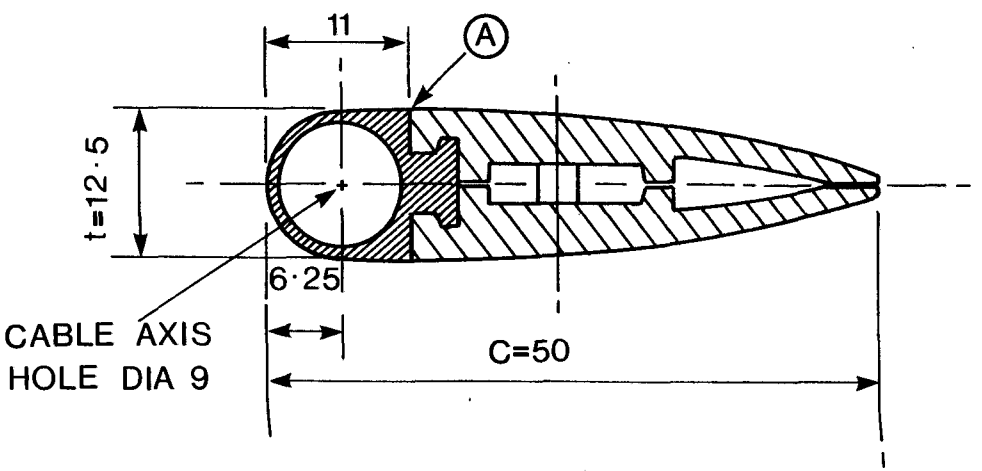

Not to scale
Dimensions in millimetres

Fig. 2 Variation in C_L, C_D, C_M with incidence for the Fathom fairing. Wind tunnel results V = 40 m/s, Re = 2.08×10^5, no end plates, aspect ratio = 10. (ref. Henderson (1978))

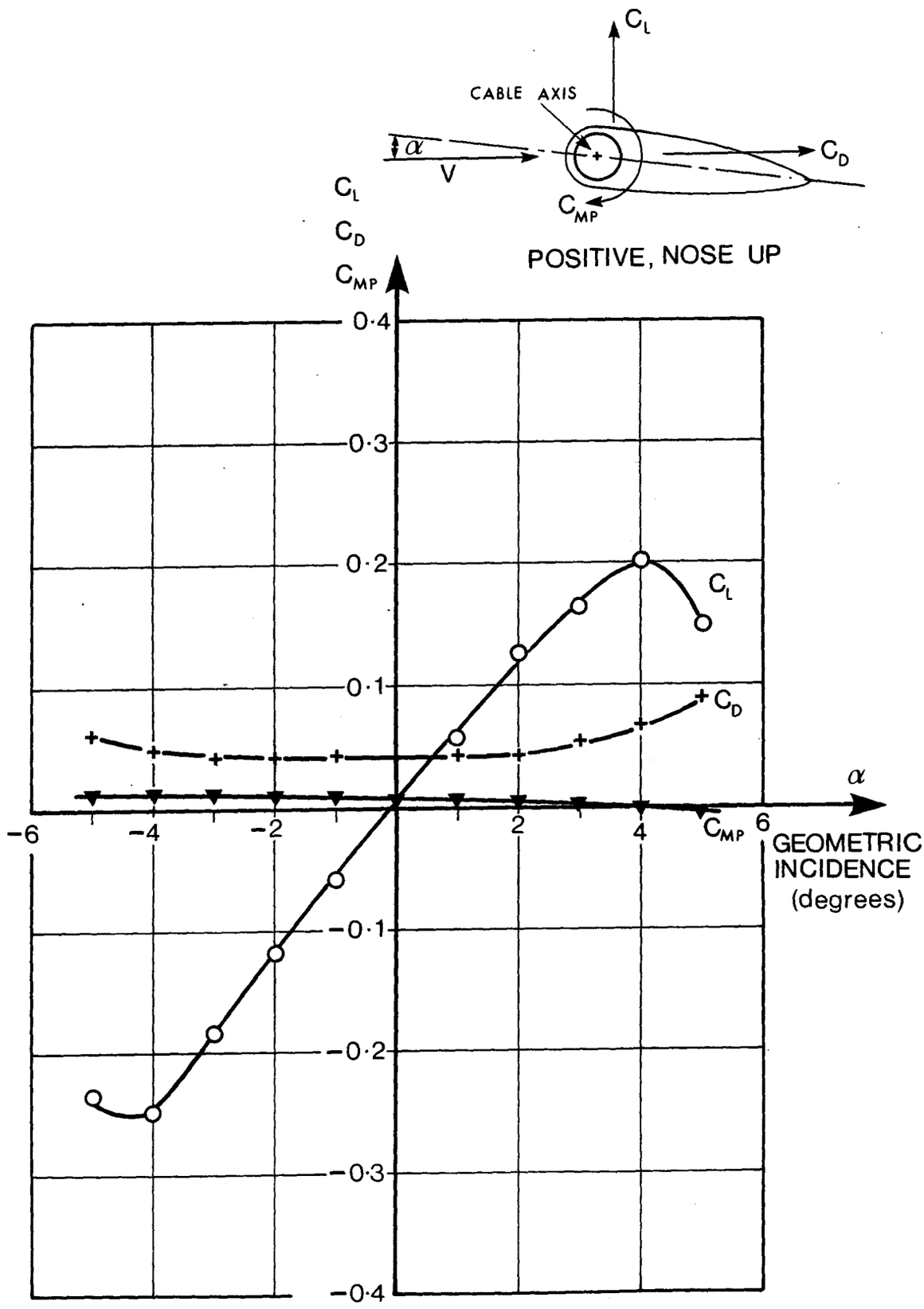

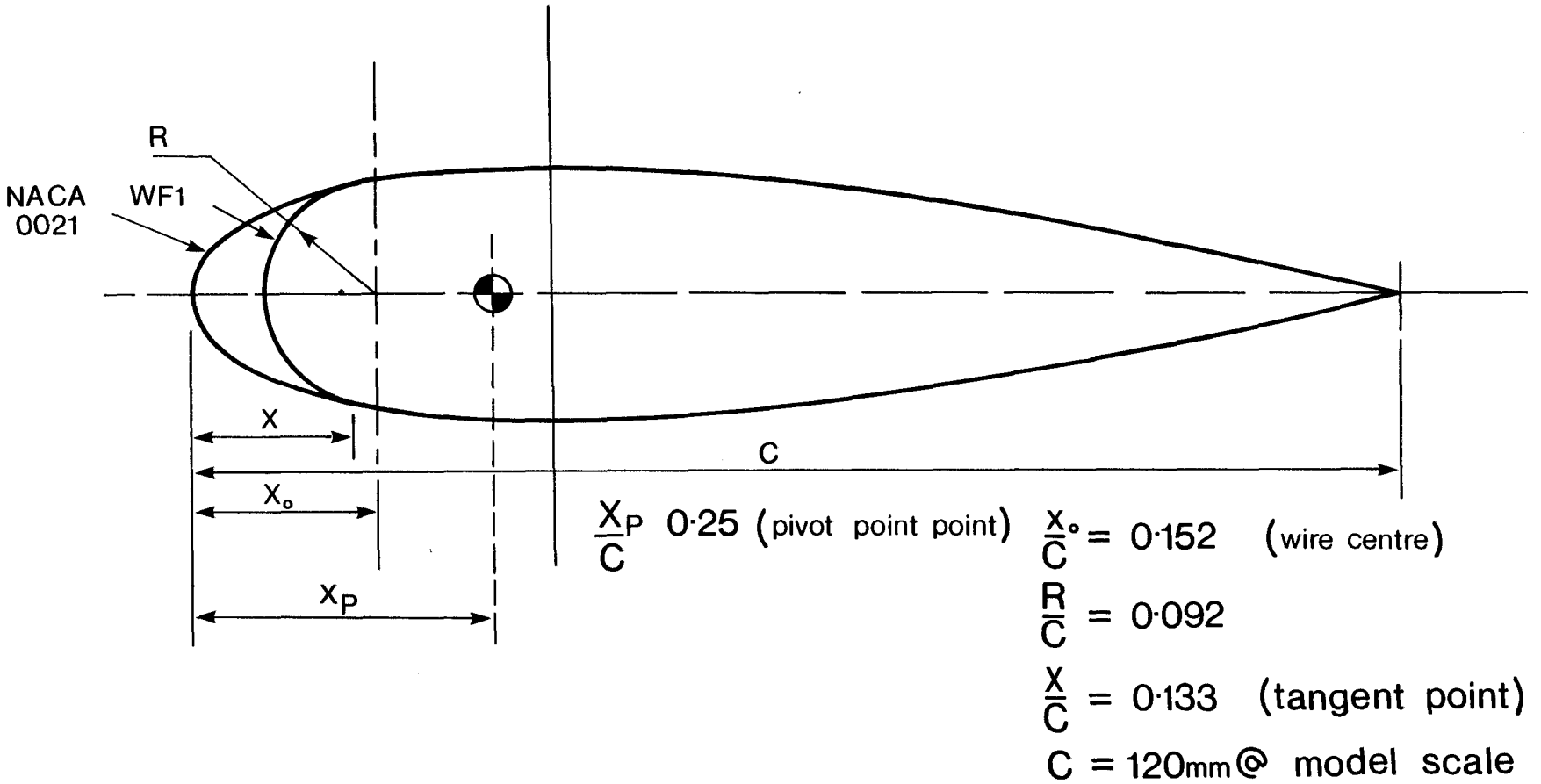

Fig. 3 Section geometries for the NACA 0021 and WF1 wind tunnel models

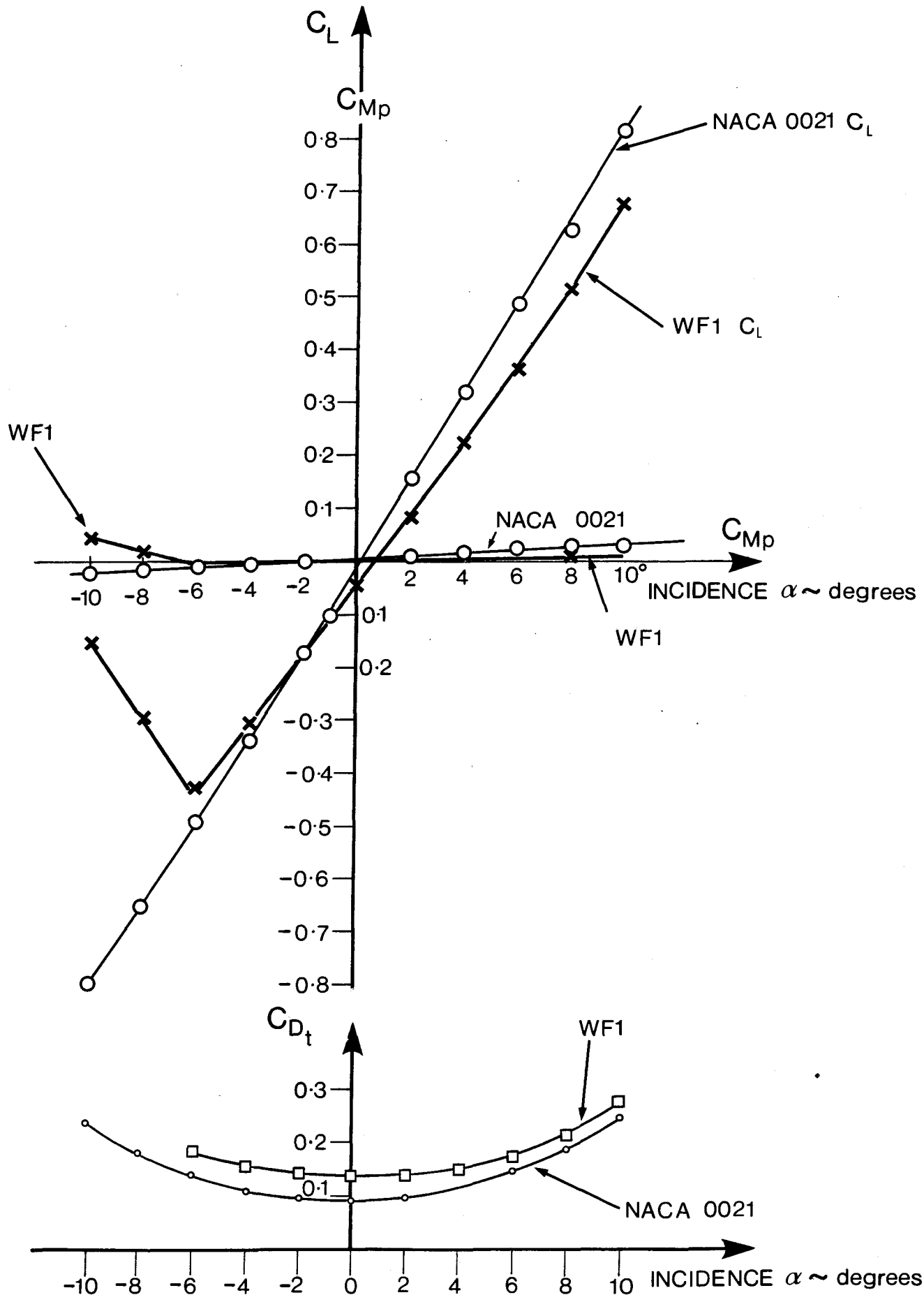

Fig. 4 Variation of lift, drag and pitching moment coefficients with incidence for NACA 0021 and WF1 sections as measured in the Bath University wind tunnel

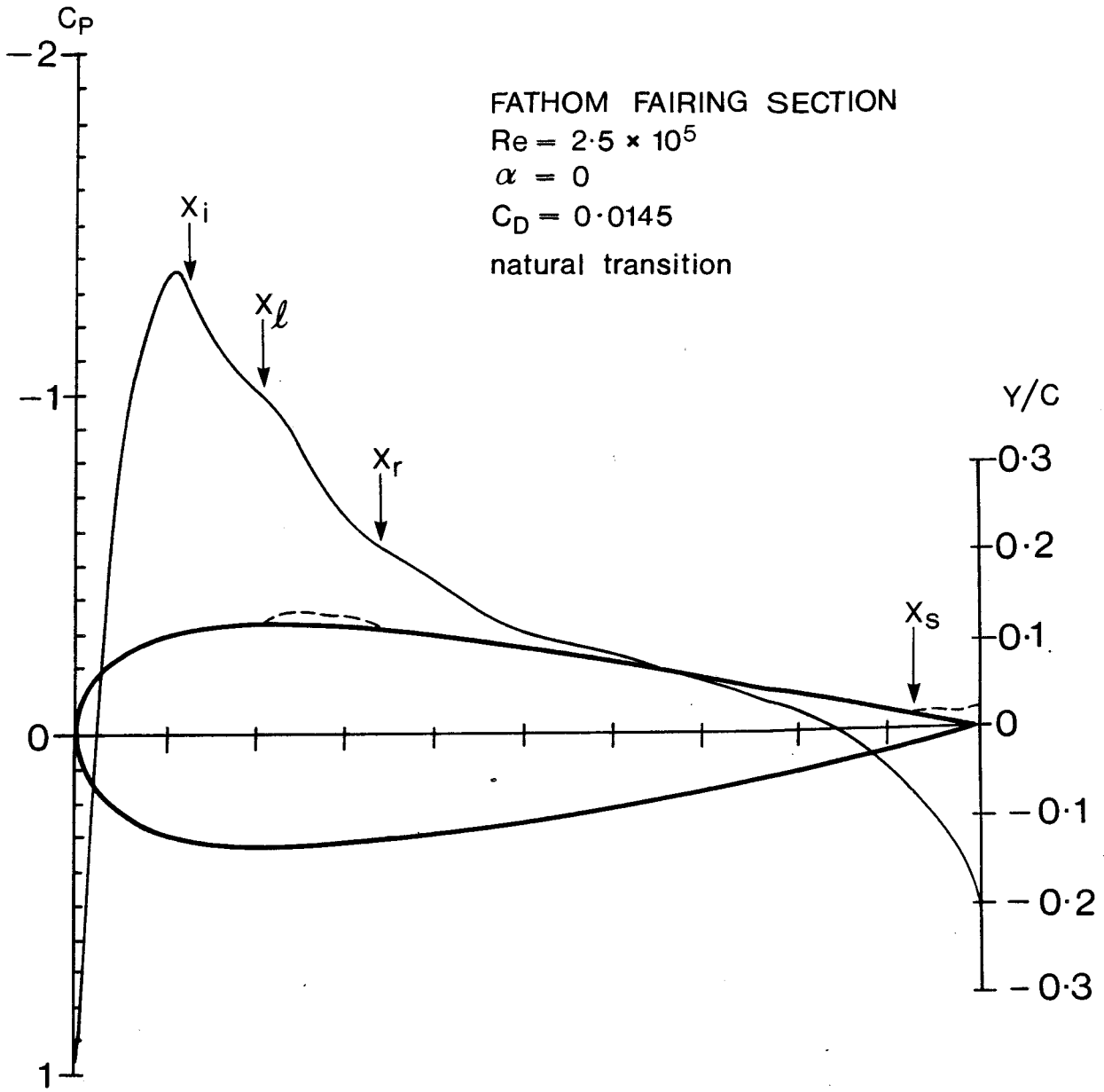

Fig. 5 Inviscid pressure distribution and schematic boundary layer behaviour as predicted by the simplified analysis program

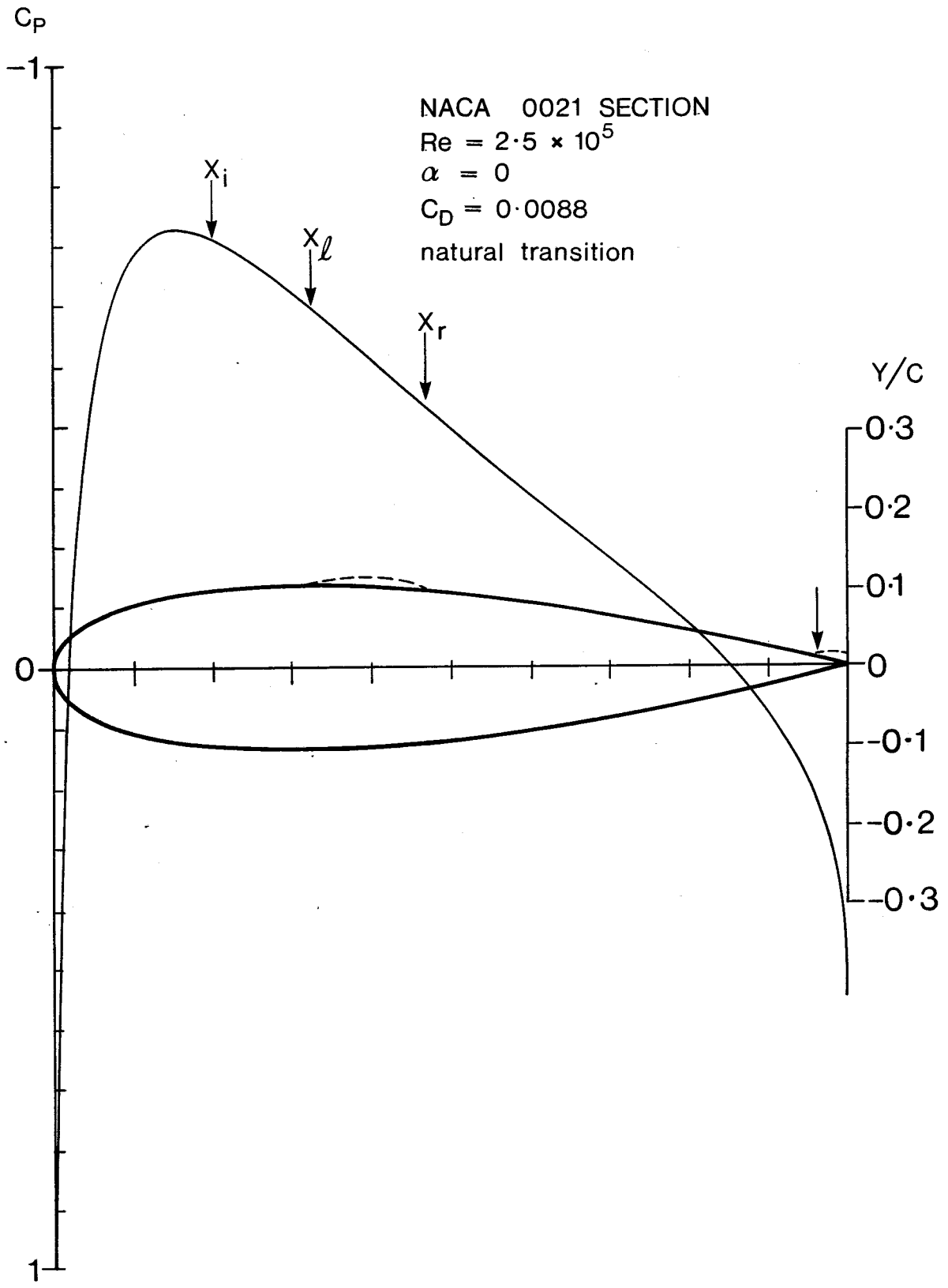

Fig. 6 for caption see fig. 5

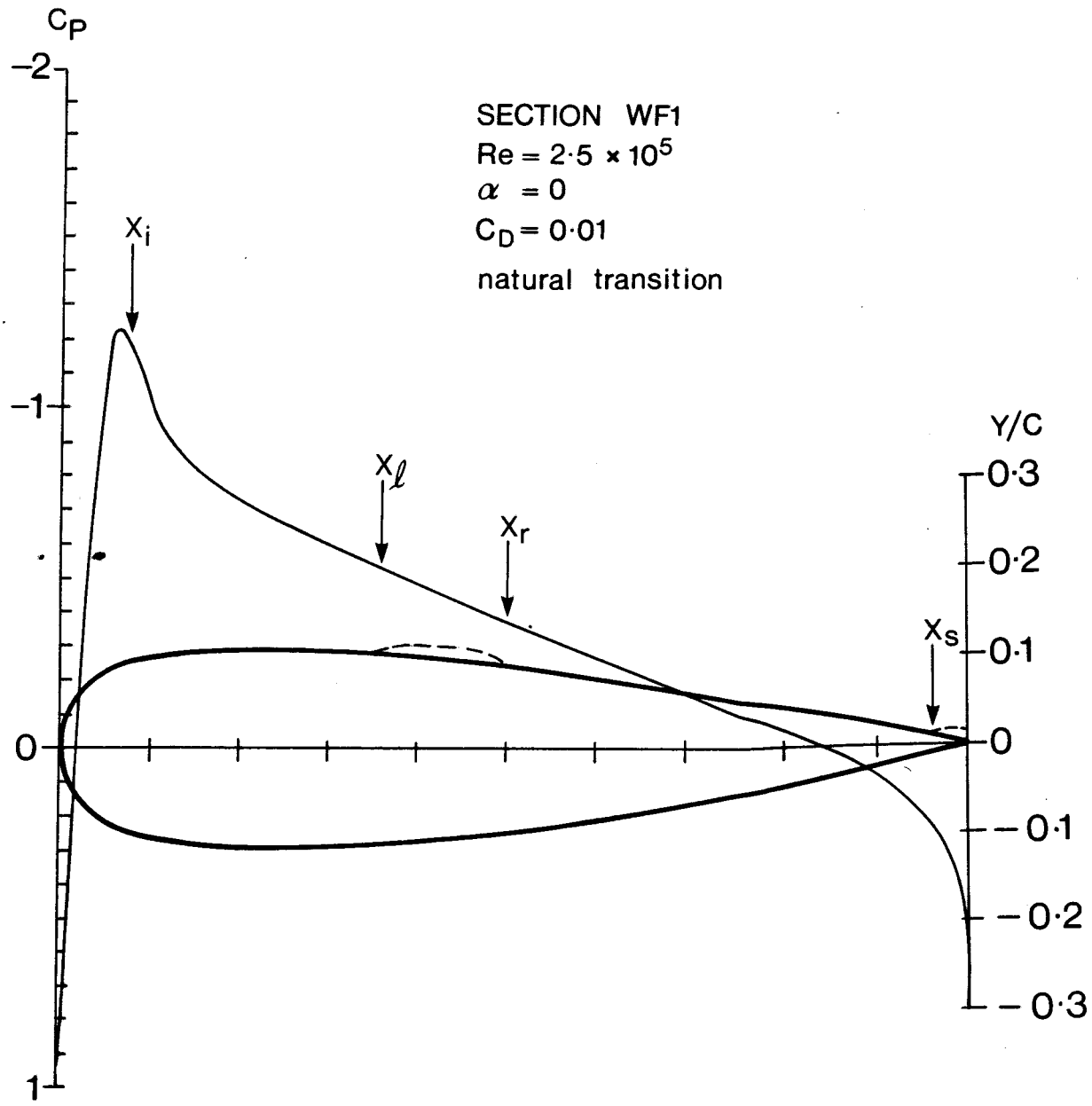

Fig. 7 for caption see fig. 5

Fig. 8 Design solution WF2

t = 0.213 at x = 0.273

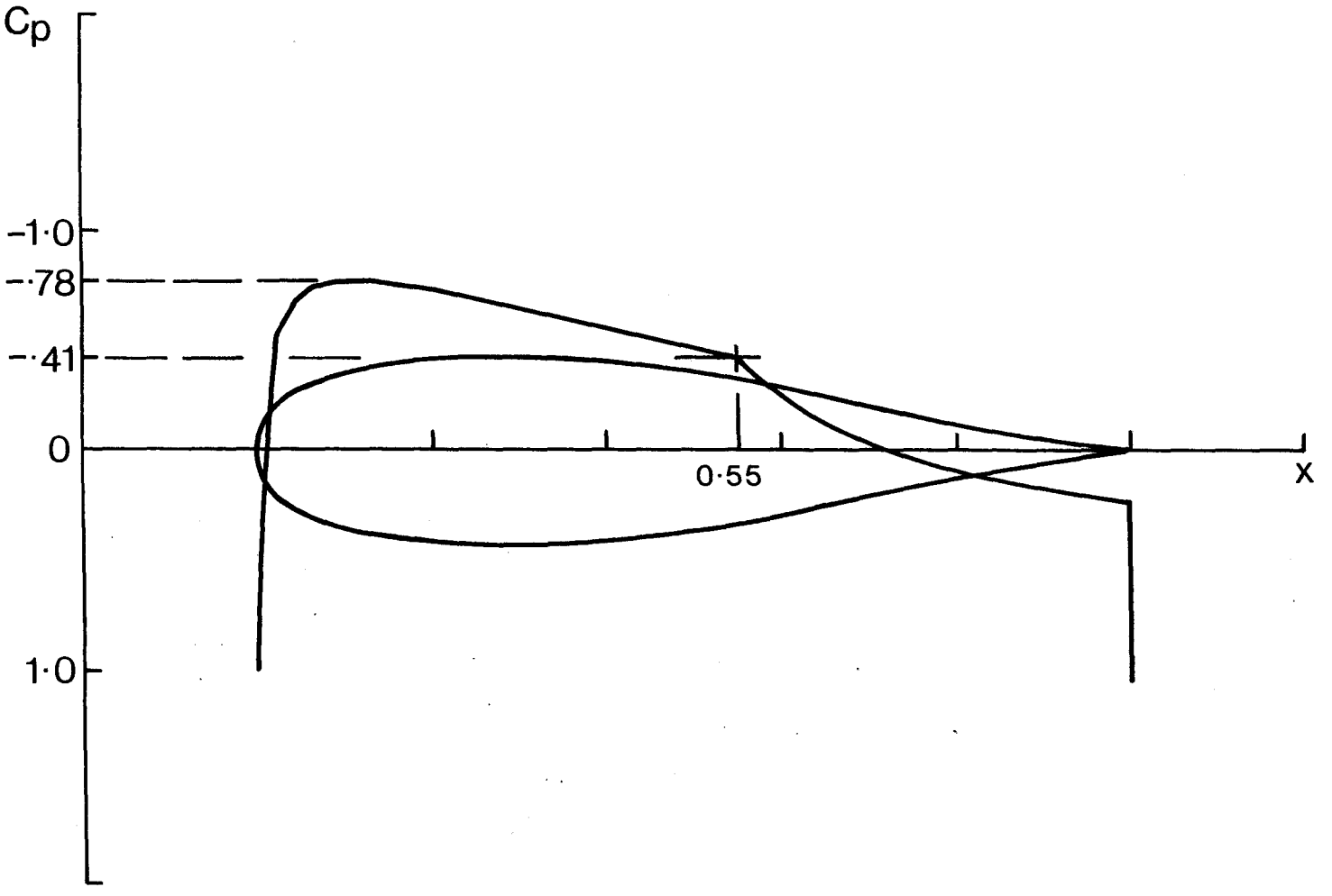

Fig. 9 Design solution WF5

t = 0.2 at x = 0.295

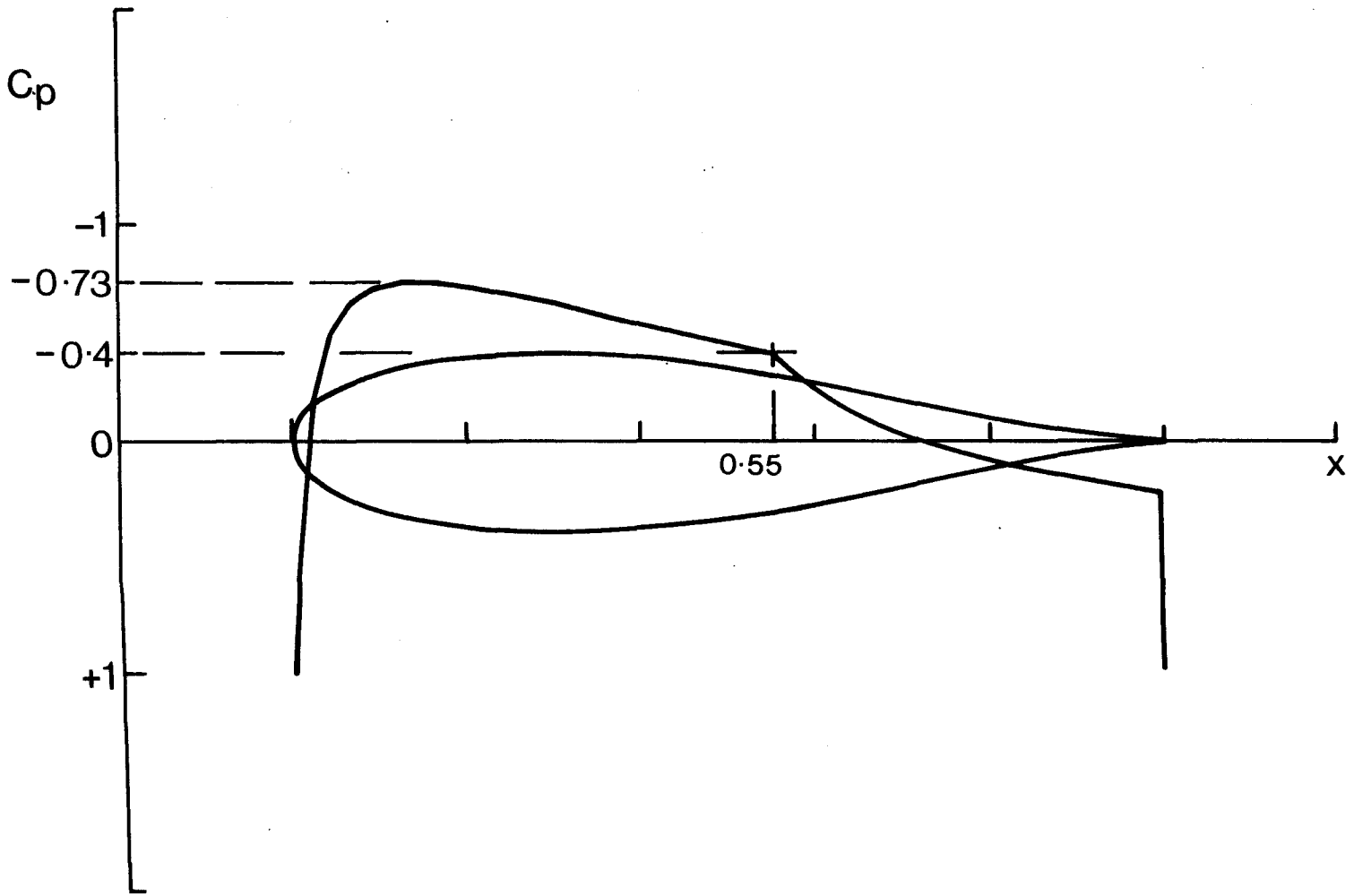

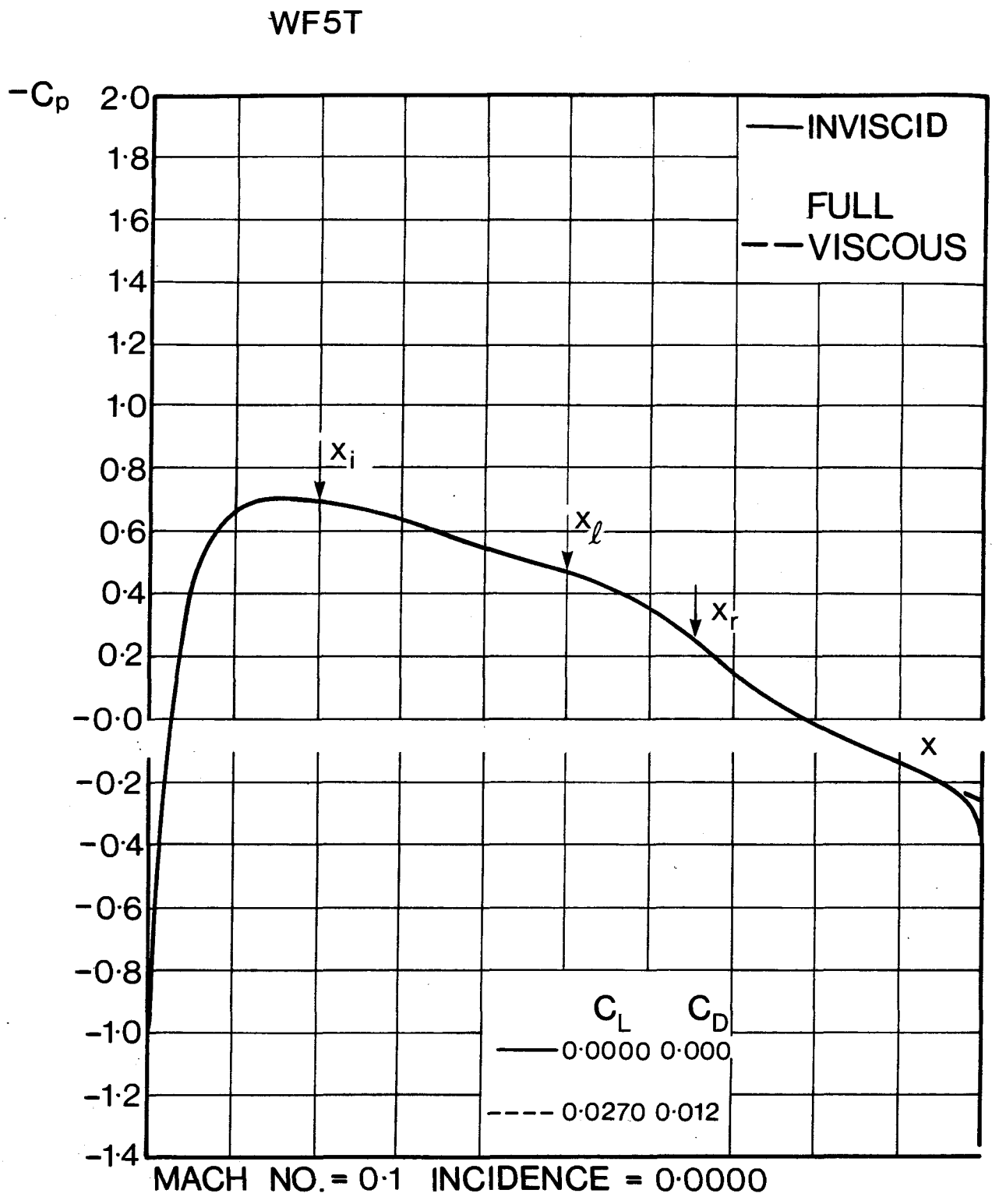

x_i initial boundary layer instability detected

x_ℓ laminar separation point

x_r reattachment point

x_s turbulent separation point

Fig. 10a Numerically predicted pressure distributions for the inviscid and full viscous solutions for section WF5T at Re = 2.5 x 10^5 with transition fixed at x = 0.5

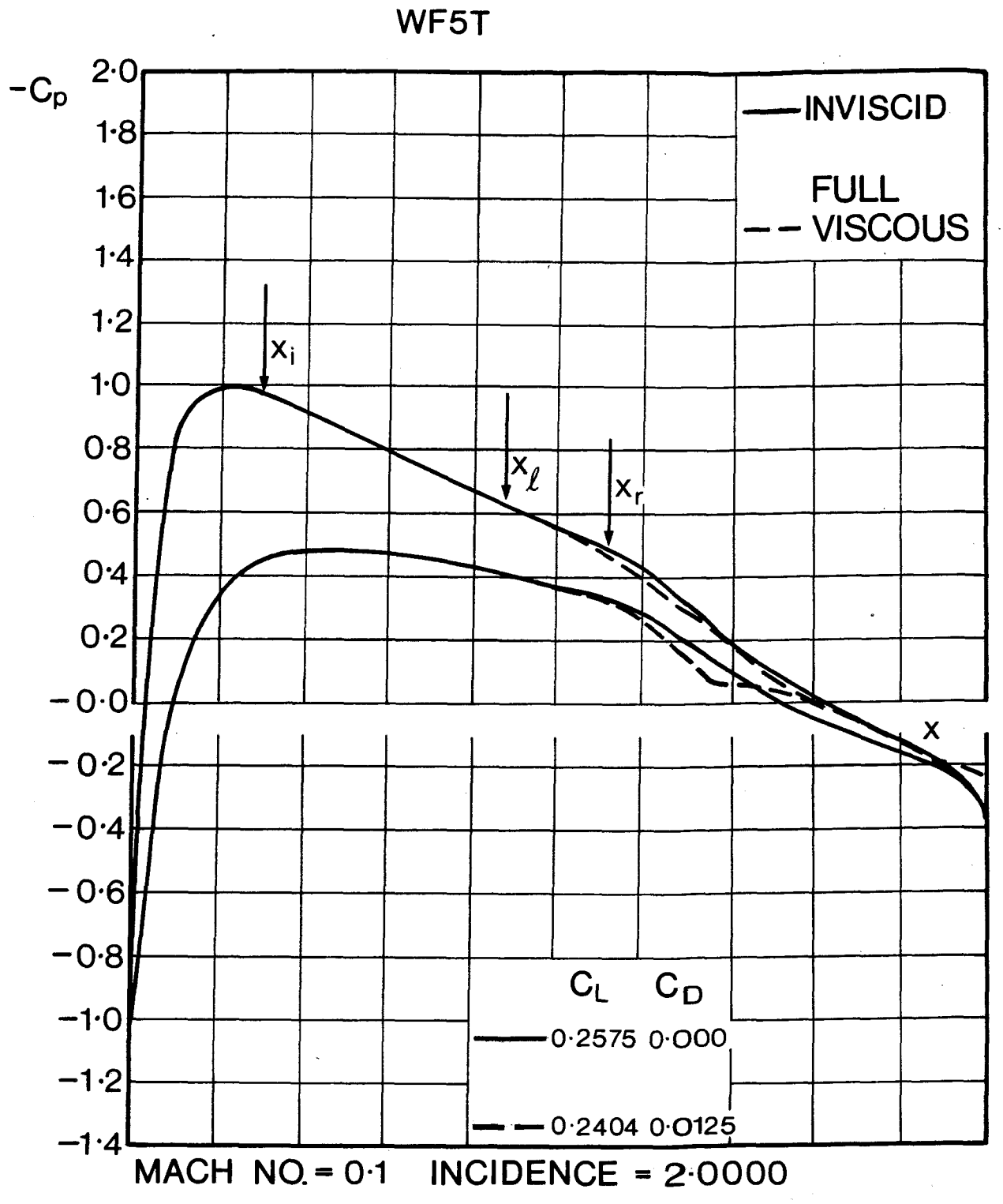

Fig. 10b for legend see fig. 10a

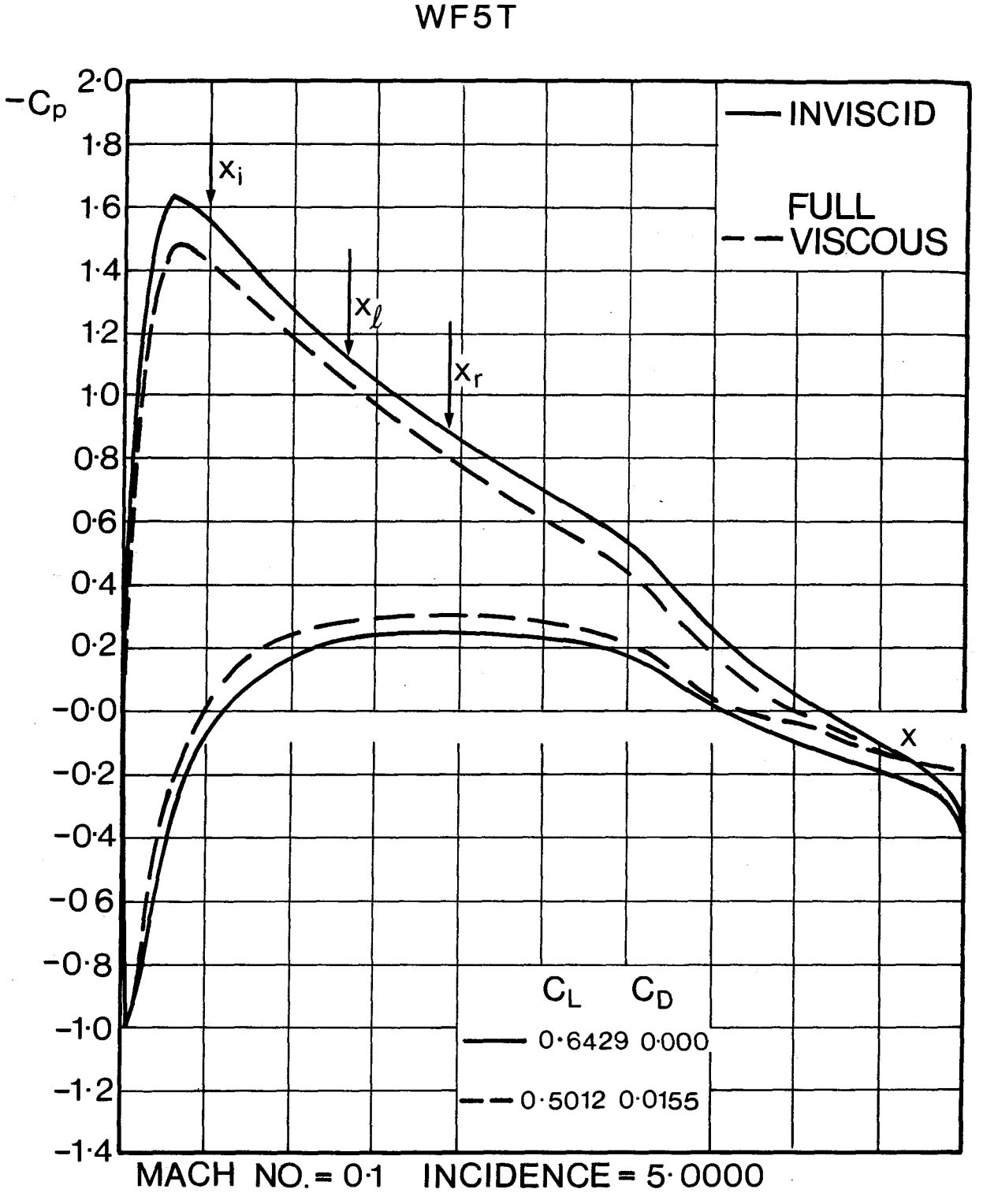

Fig. 10c for legend see fig. 10a

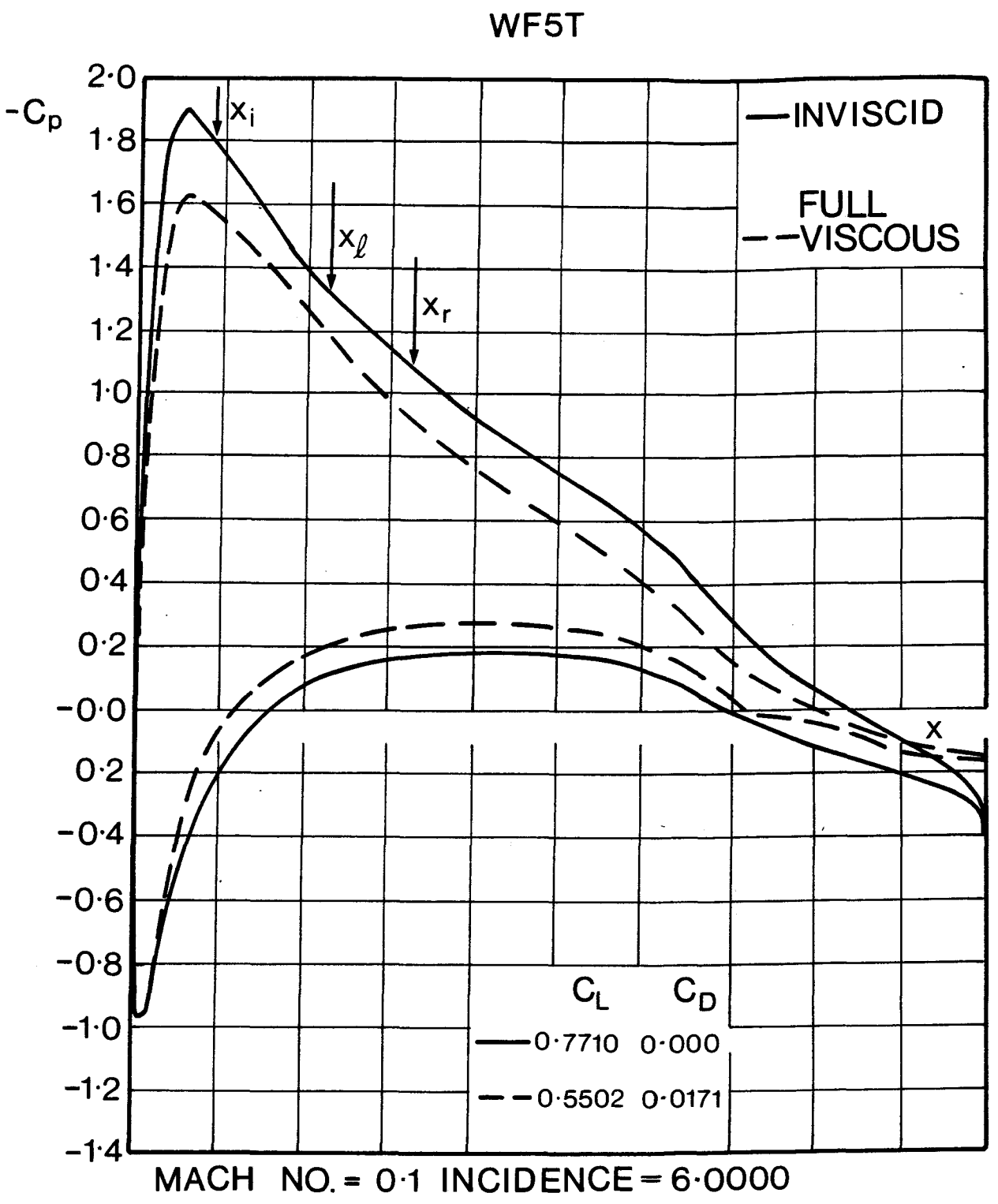

Fig. 10d for legend see fig. 10a

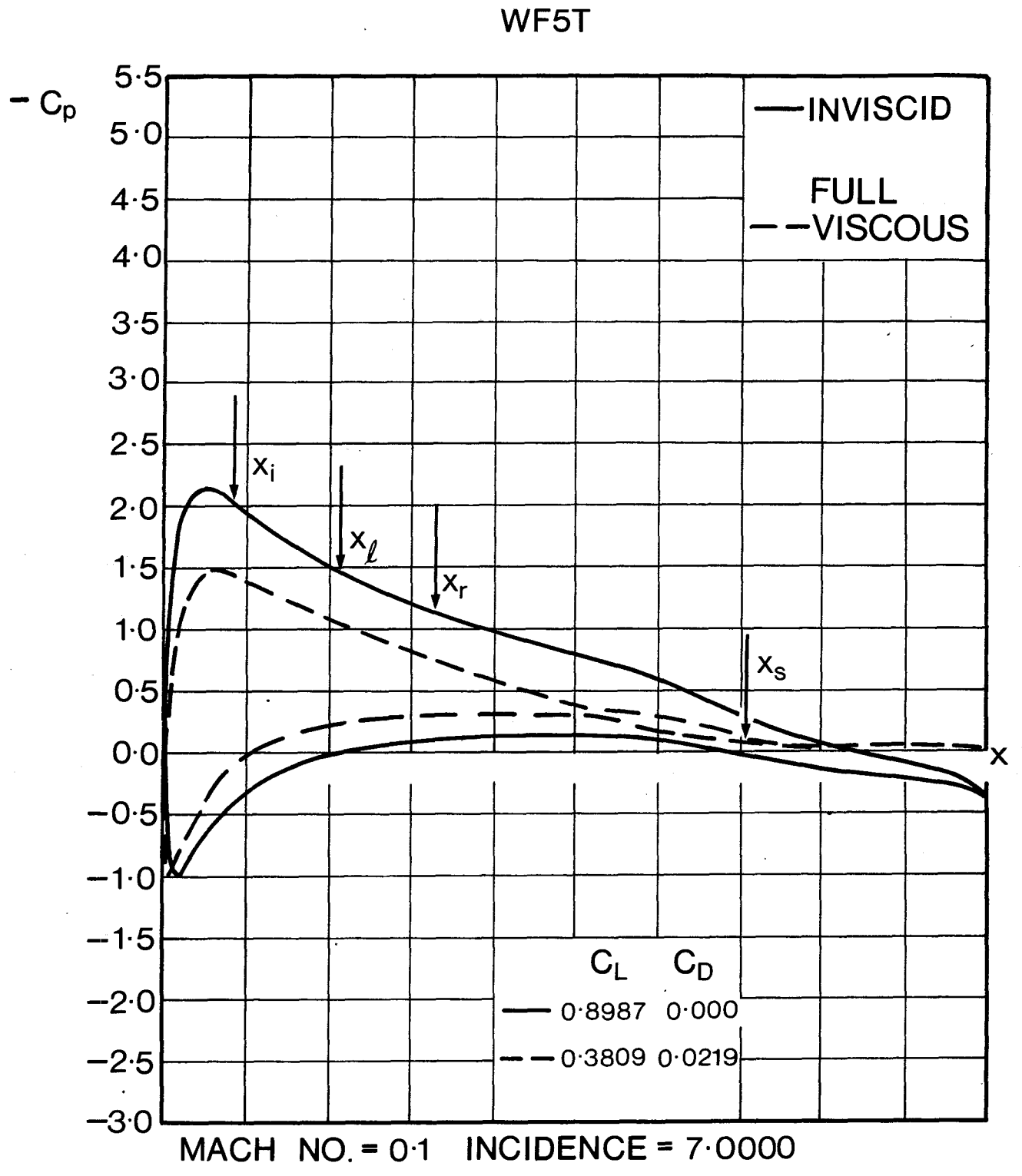

Fig. 10e for legend see fig. 10a

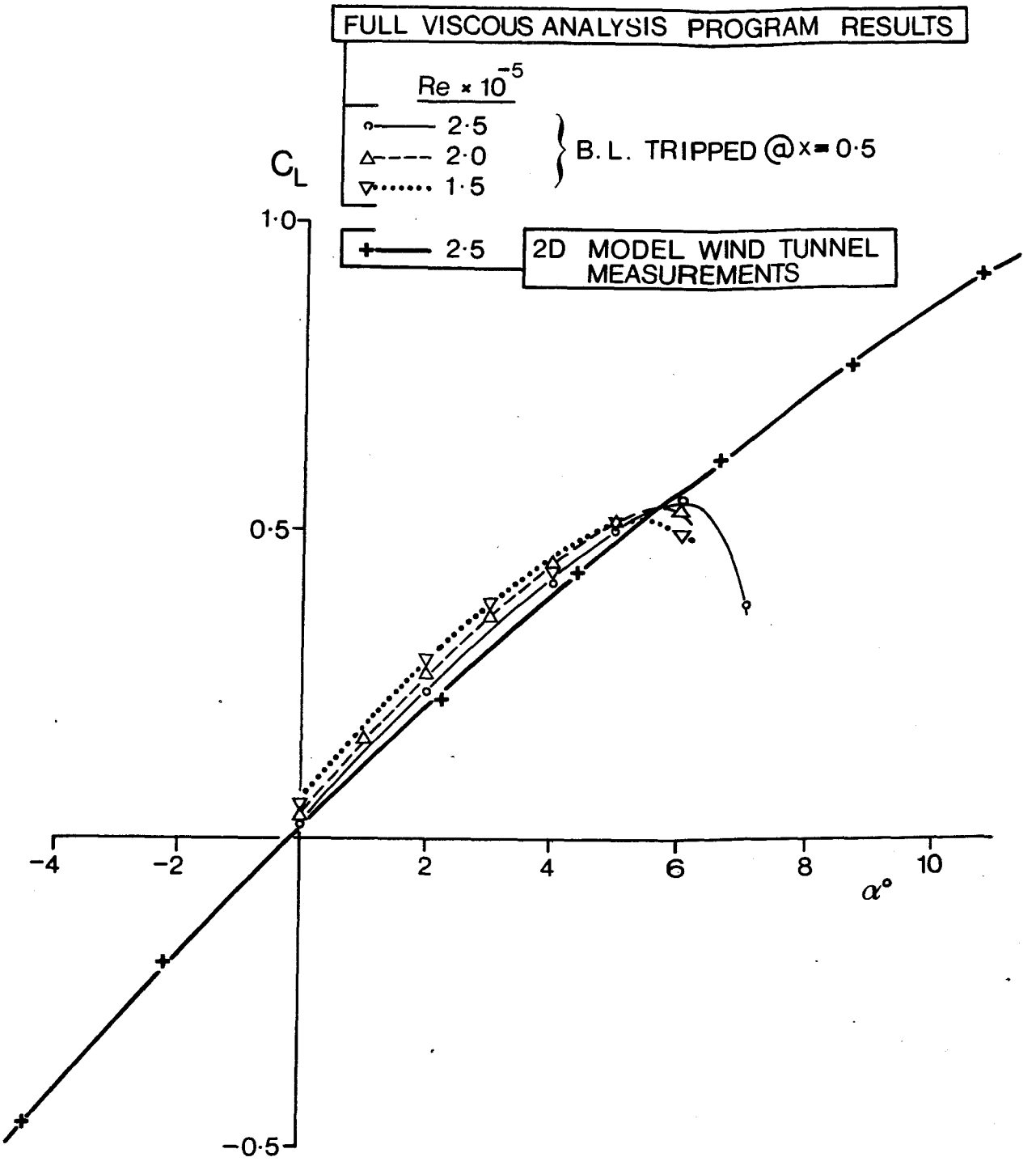

Fig. 11a Comparison of the results obtained from the full viscous analysis program with the 2D model wind tunnel measurements for section WF5T

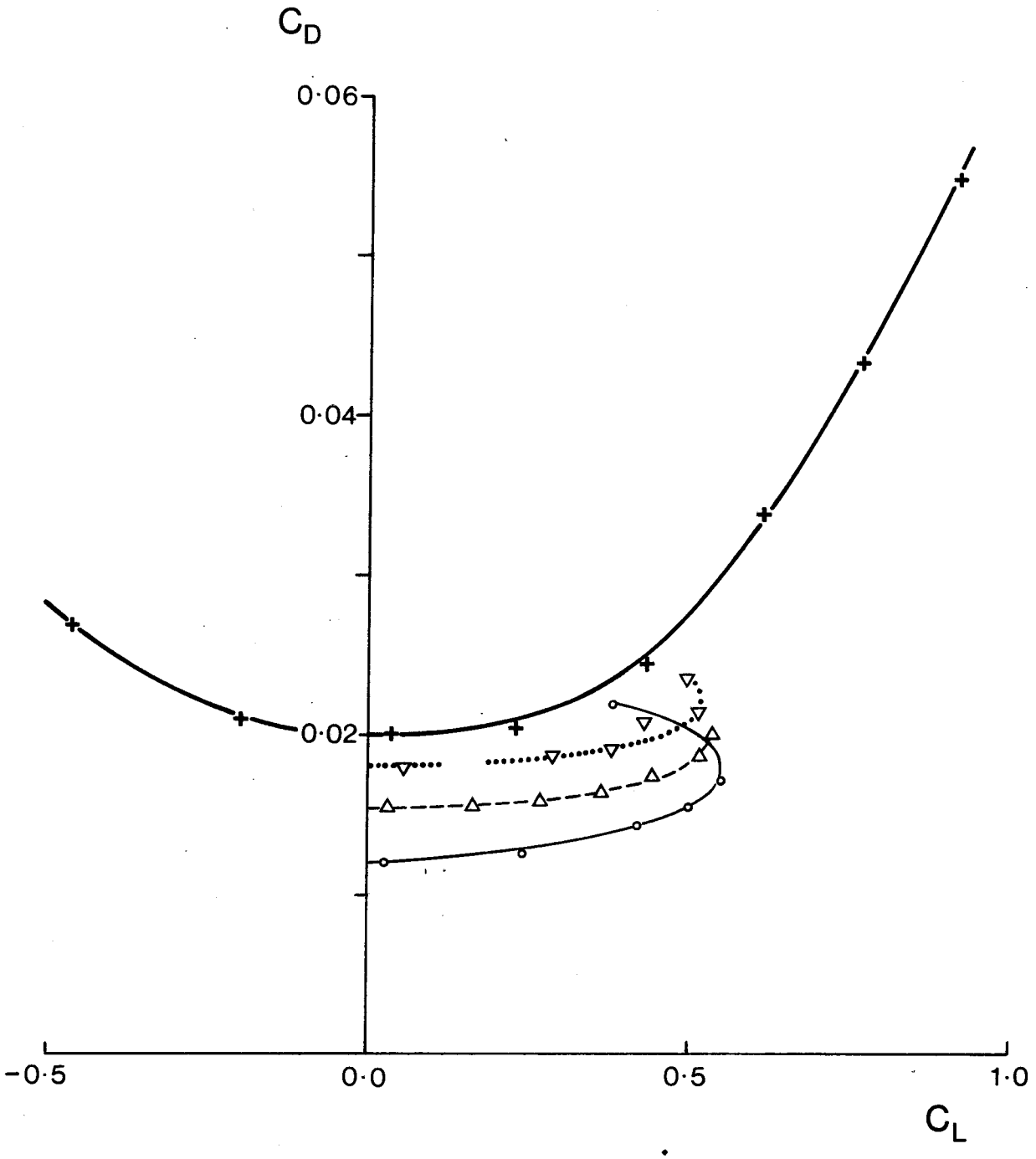

Fig. 11b for caption and legend see fig. 11a

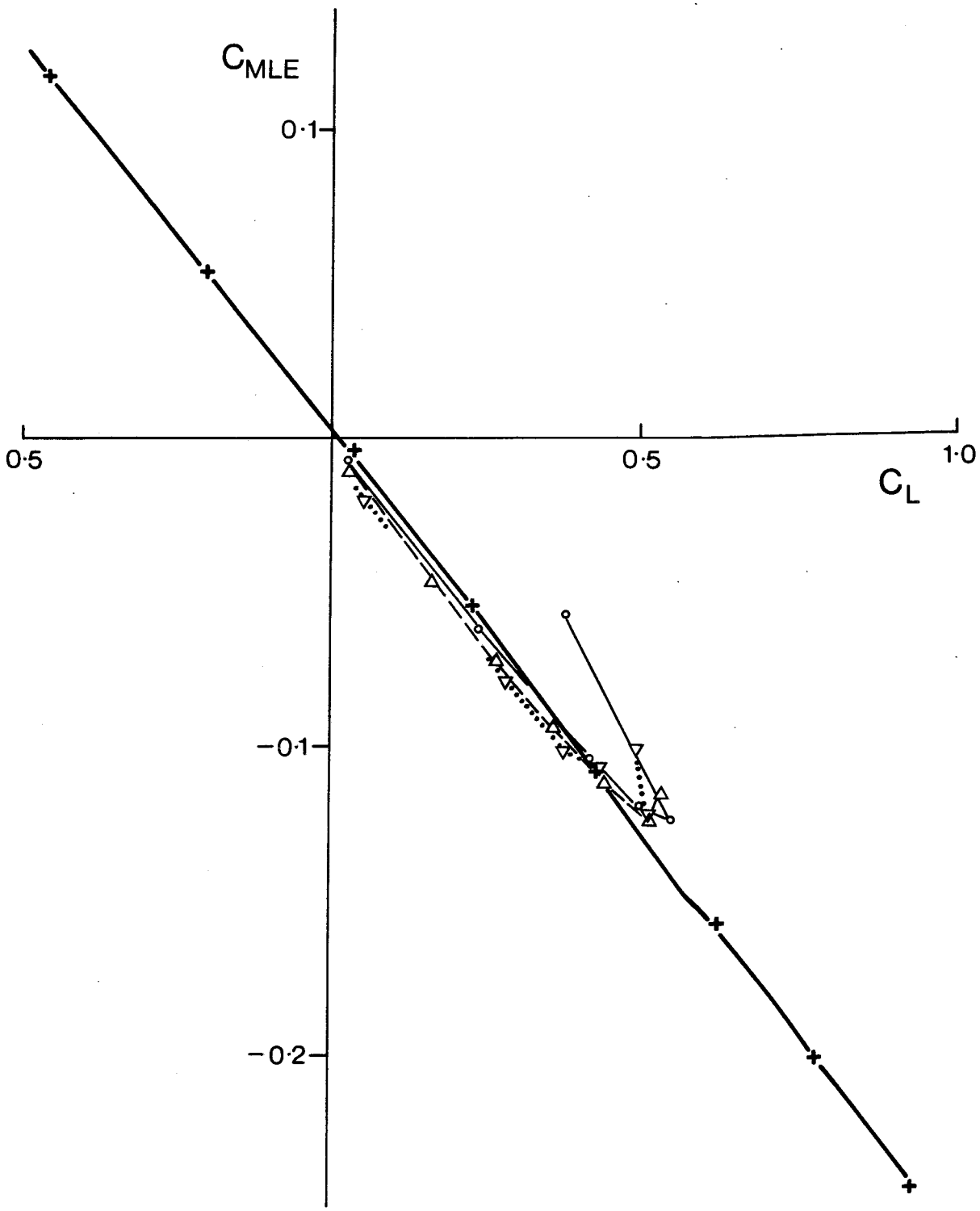

Fig. 11c for caption and legend see fig. 11a

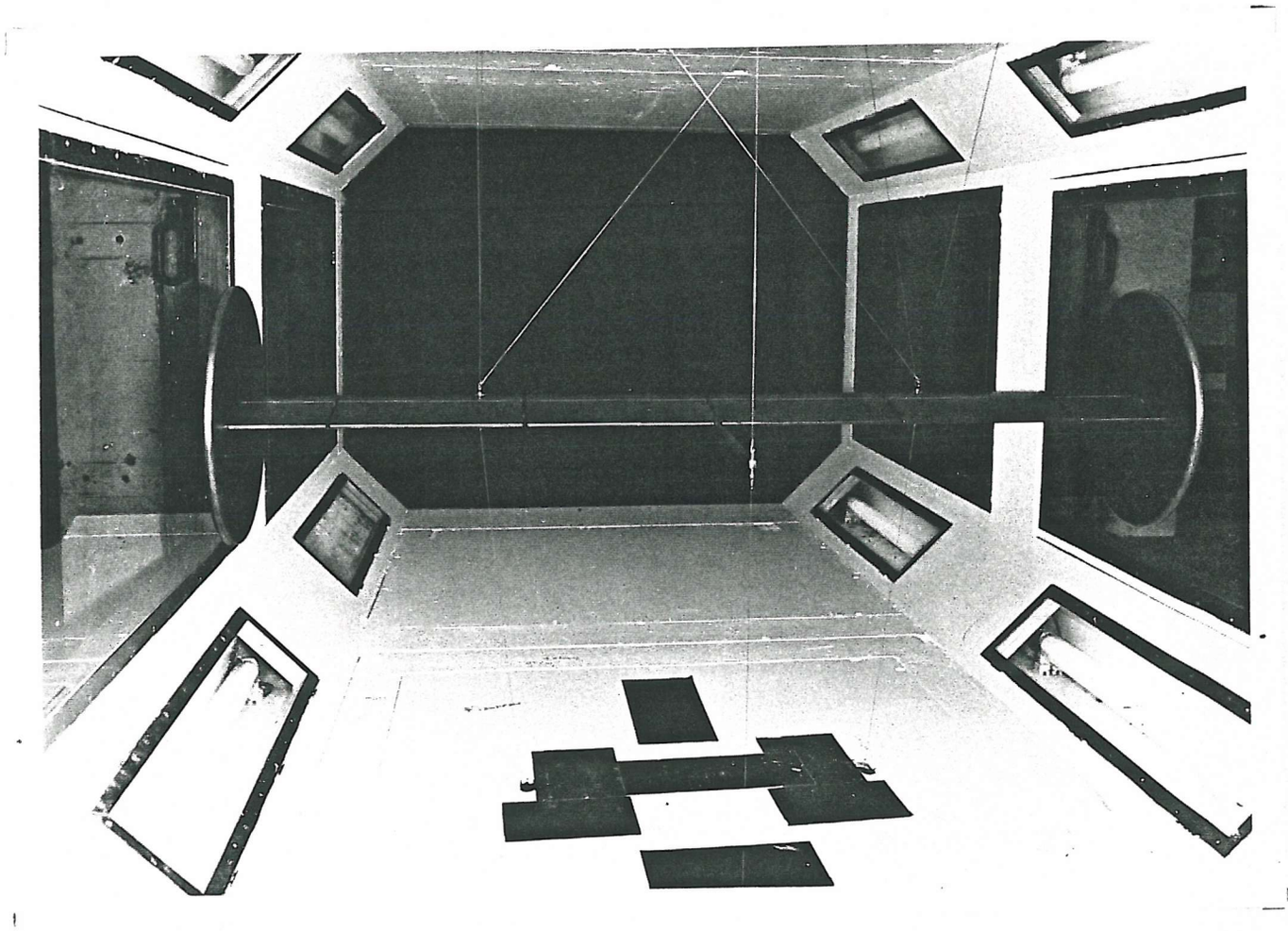

Fig. 12 The 3-dimensional fairing model mounted in the 3' x 4' wind tunnel, looking towards the tunnel contraction

Fig. 13 Flow visualization at Re = 2.5 x 10^5 on the two dimensional section

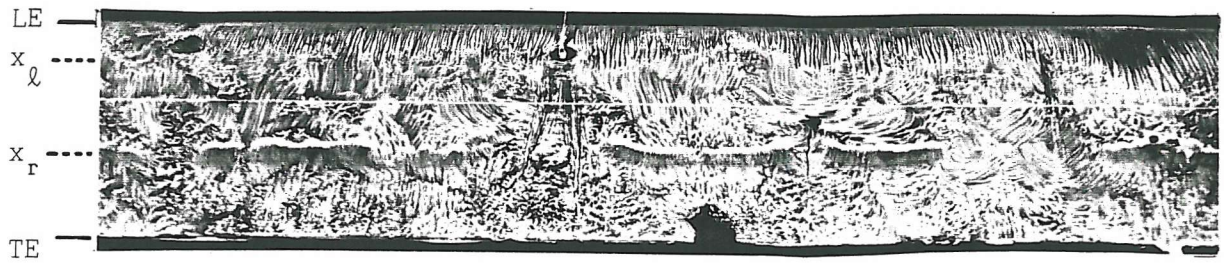

(a) $\alpha = 0°$

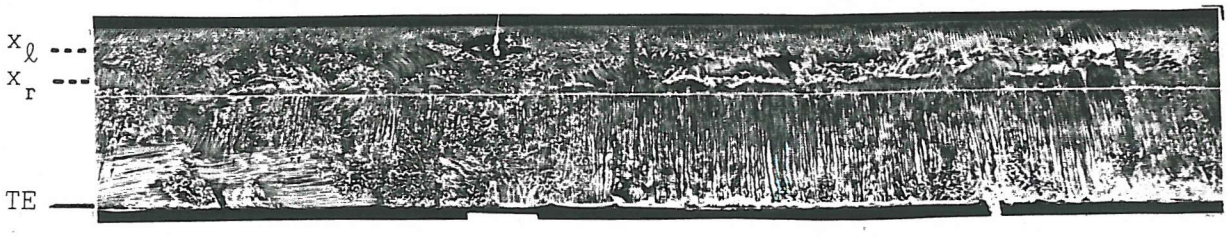

(b) $\alpha = 4°$ suction surface

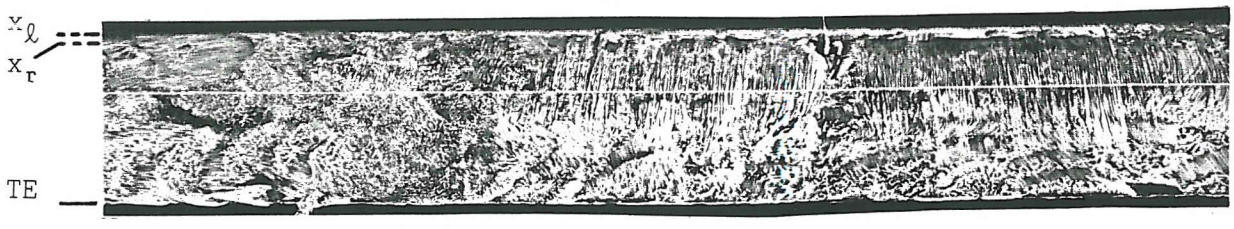

(c) $\alpha = 8°$ suction surface

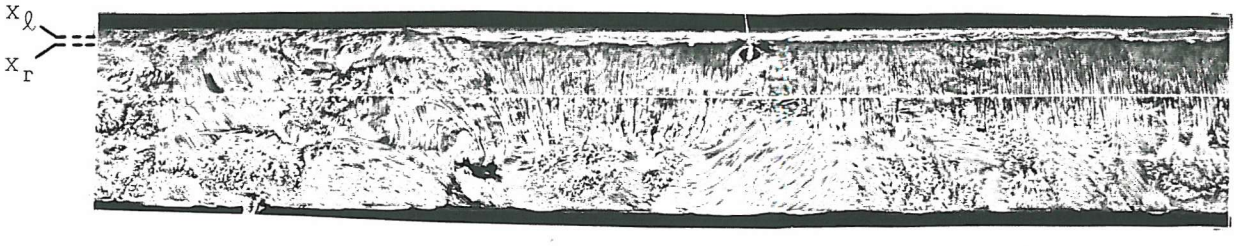

(d) $\alpha = 10°$ suction surface

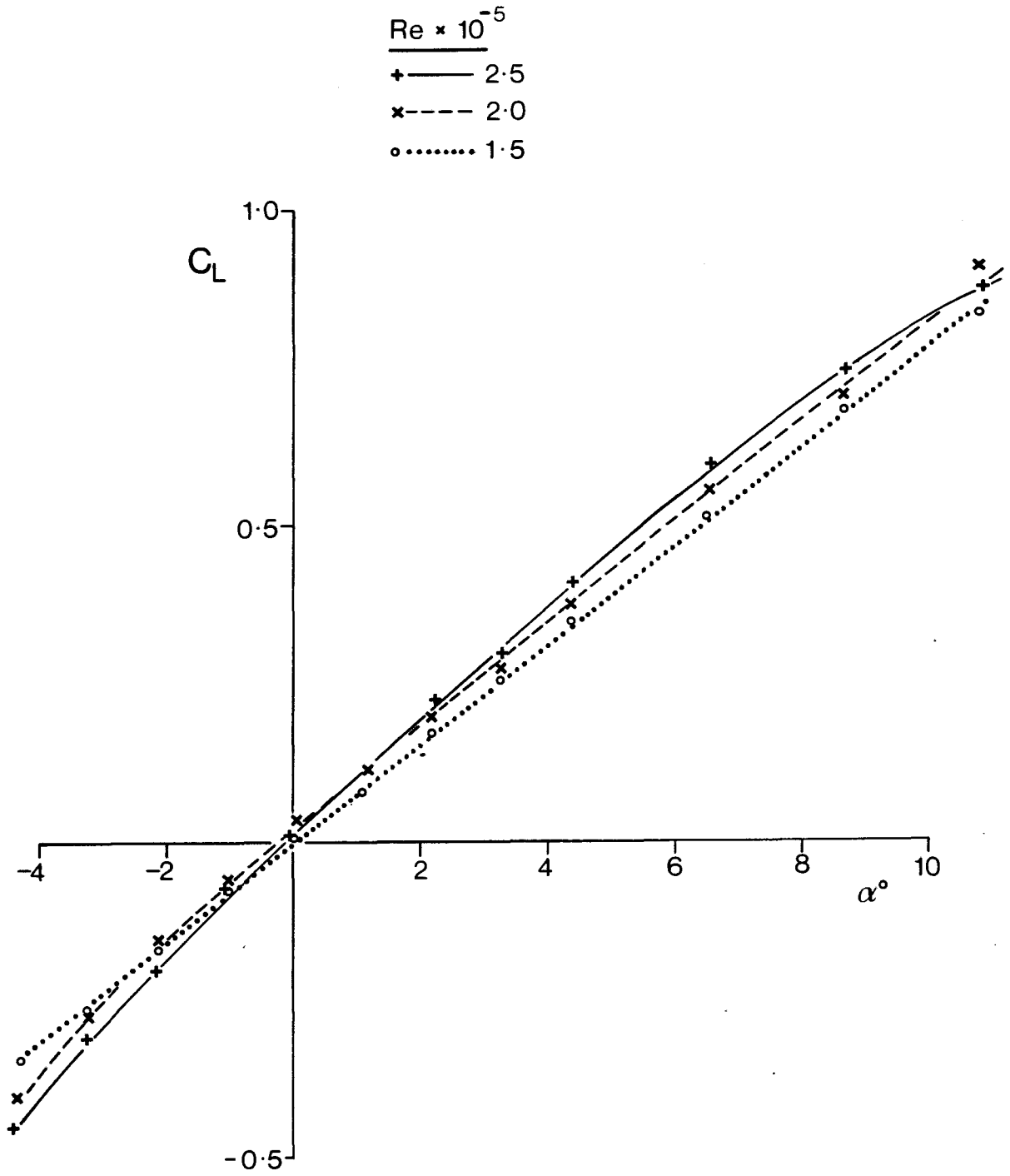

Fig. 14a Wind tunnel results for the 3D model, section WF5T

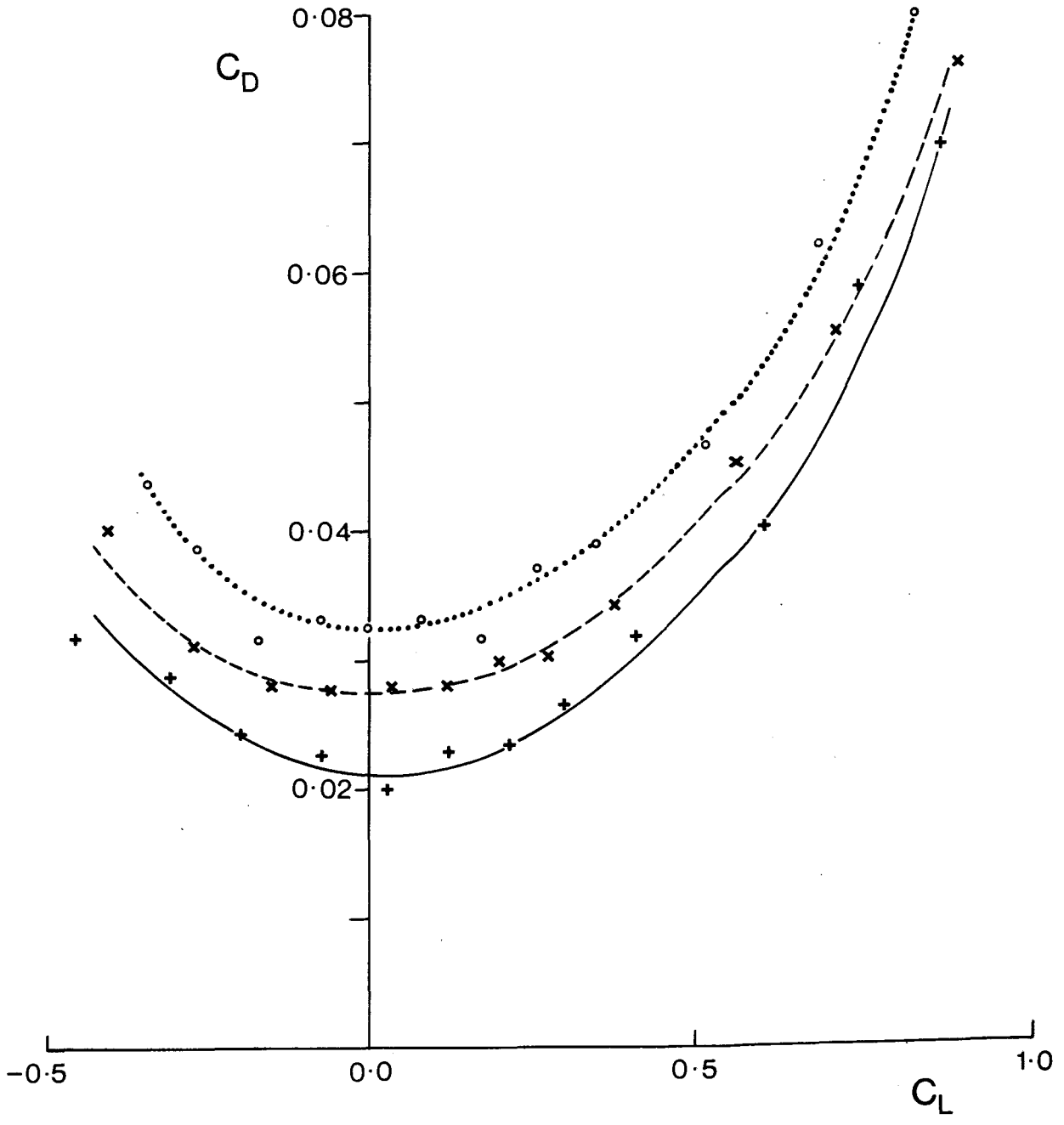

Fig. 14b for caption and legend see fig. 14a

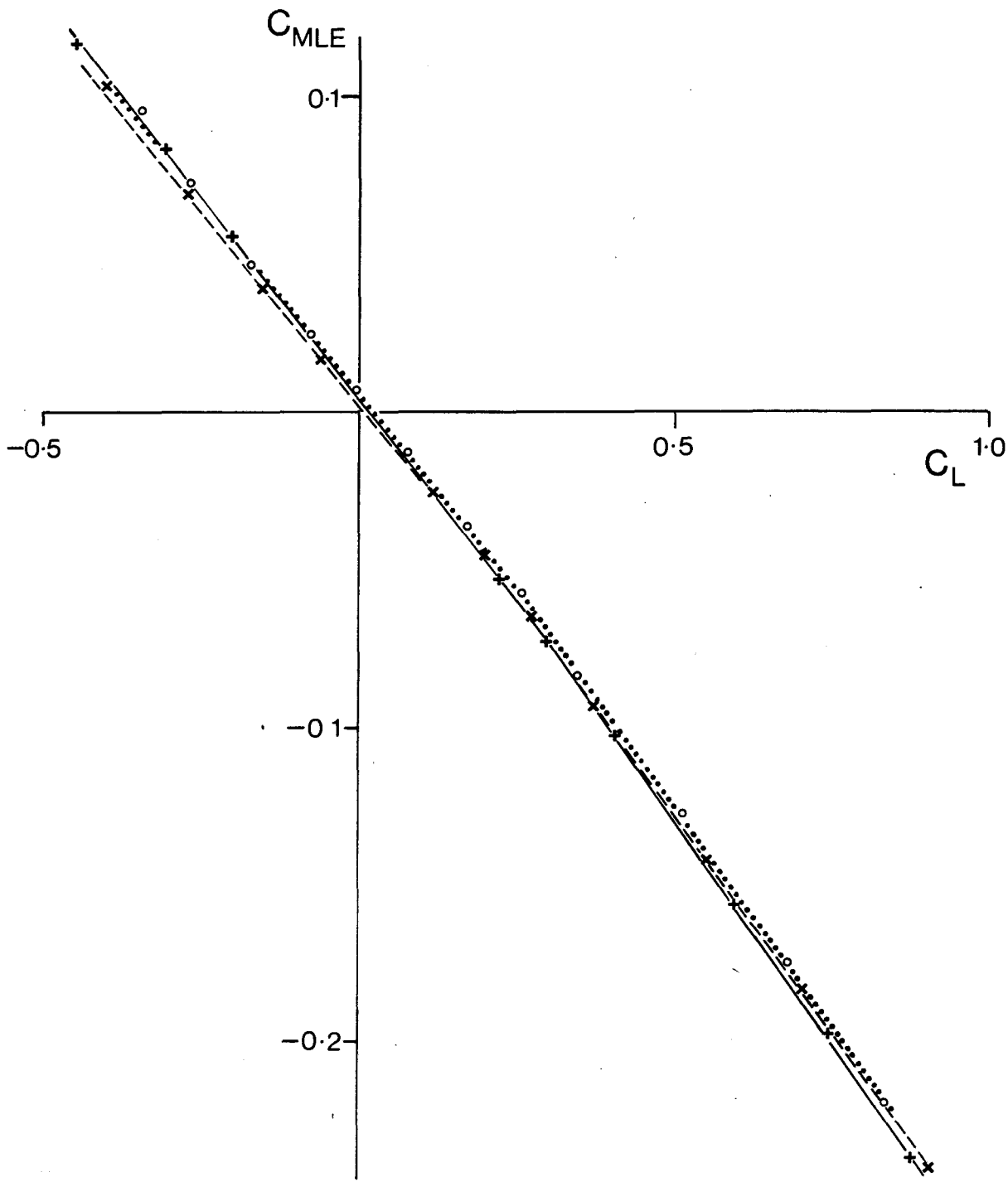

Fig. 14c for caption and legend see fig. 14a

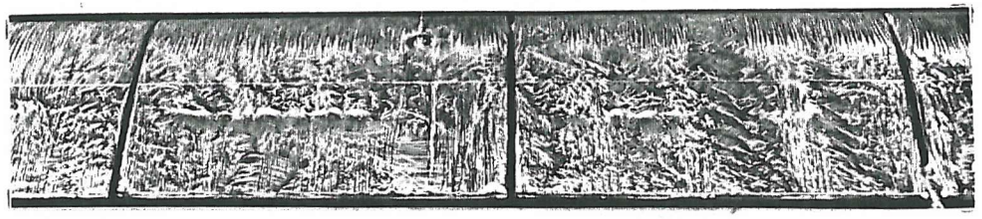

(a) α = 0° oil flow method

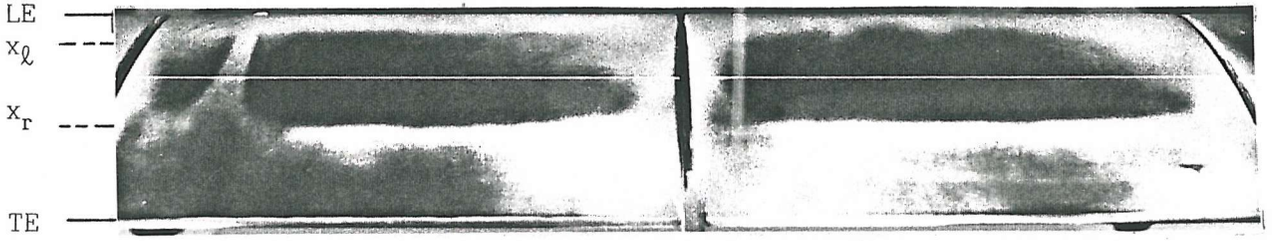

(b) α = 0° under surface, china clay method

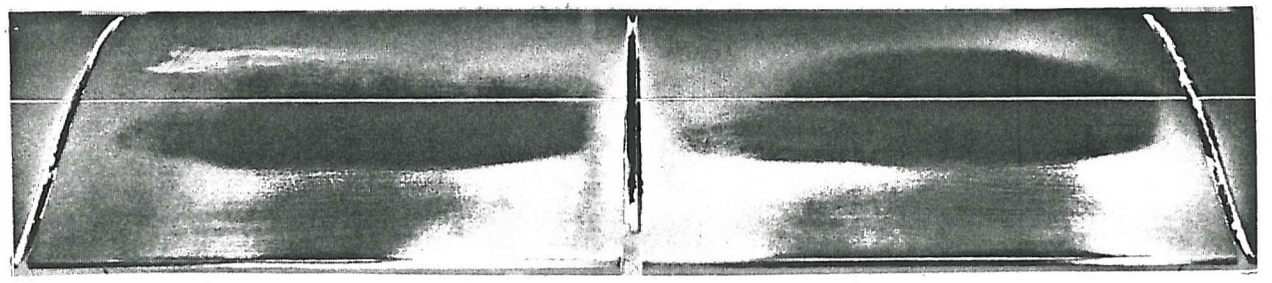

(c) α = 0° upper surface, china clay method

Fig. 15 3-Dimensional fairing flow visualization at Re = 2.5 x 10^5

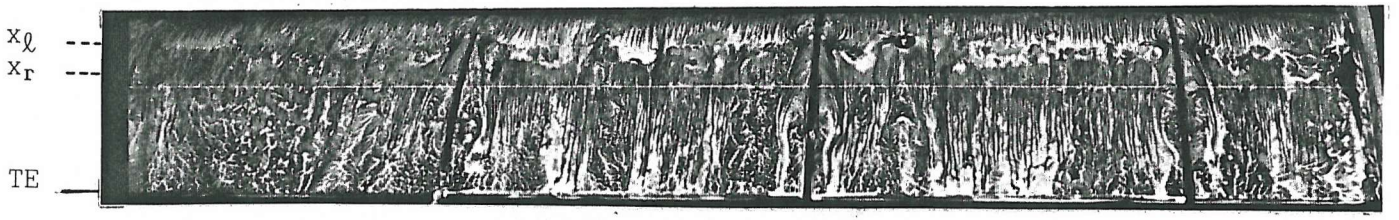

(d) α = 4° suction surface

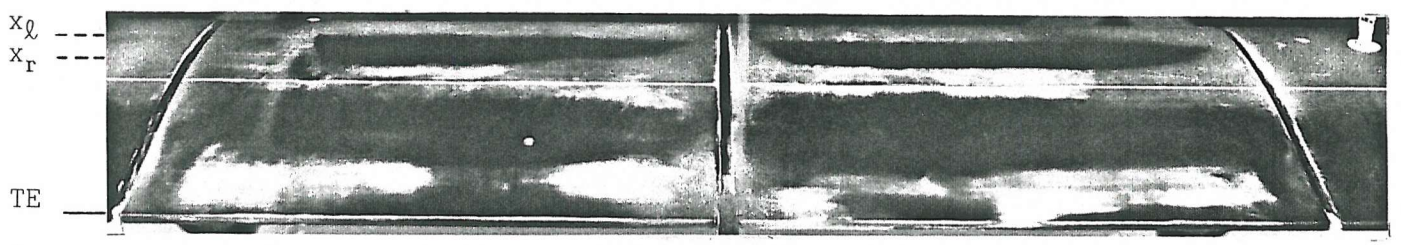

(e) α = 6° suction surface

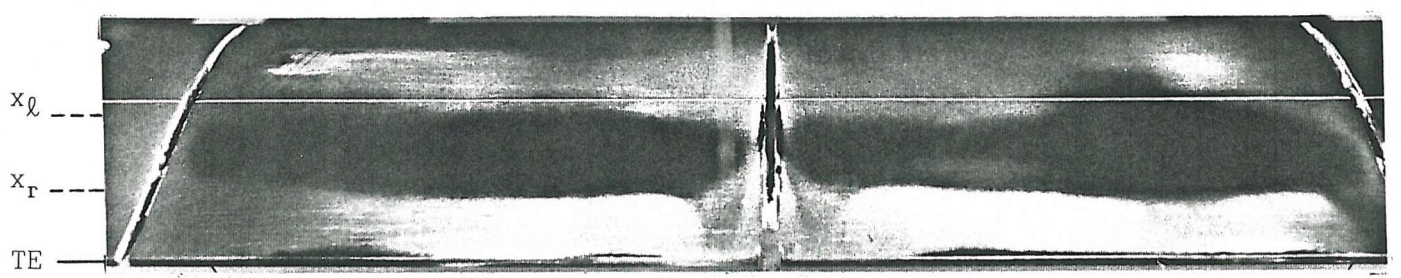

(f) α = 6° pressure surface

Fig. 15 (cont)

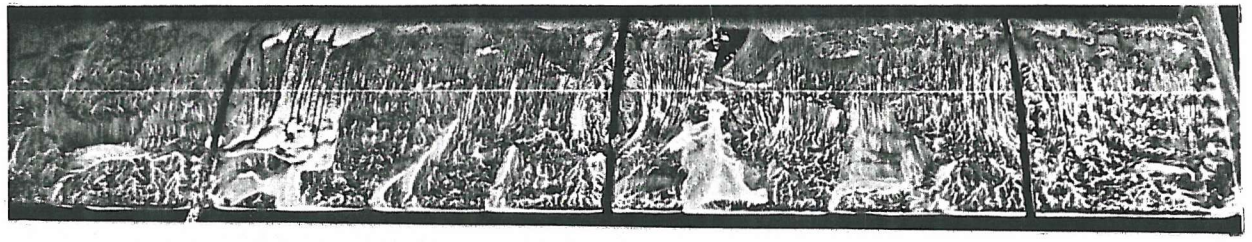

(g) α = 8° suction surface

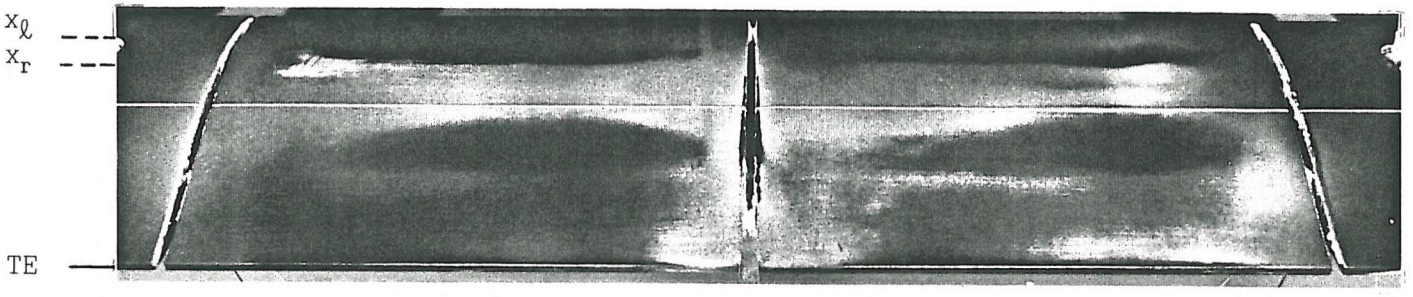

(h) α = 8° suction surface

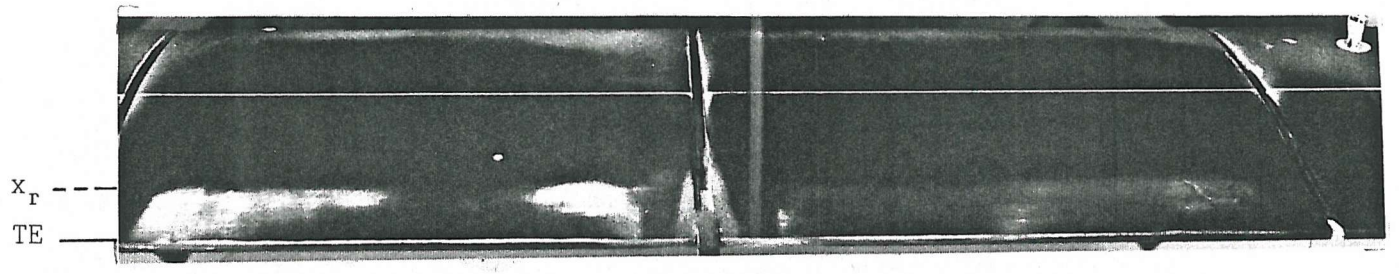

(i) α = 8° pressure surface

Fig. 15 (cont)

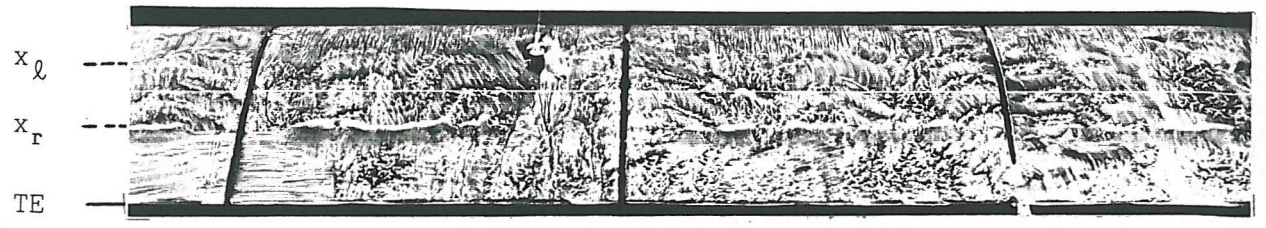

(a) α = 0° Re = 2 x 10^5

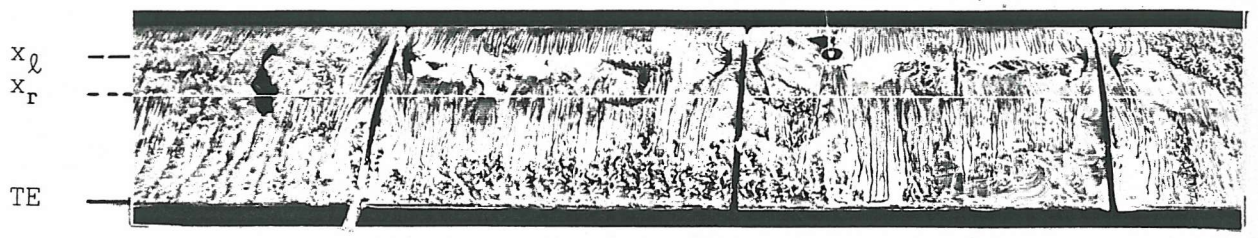

(b) α = 4° suction surface Re = 2 x 10^5

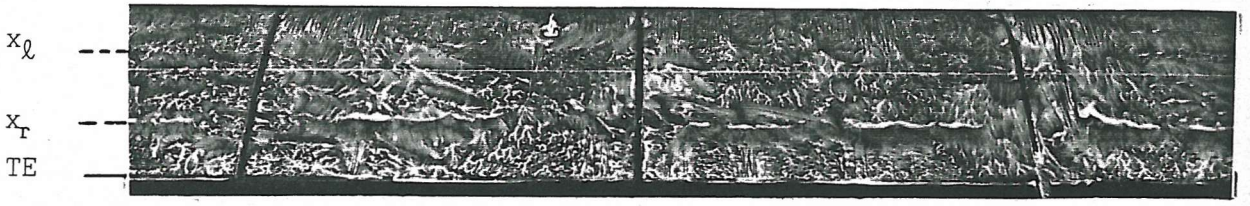

(c) α = 4° pressure surface Re = 2 x 10^5

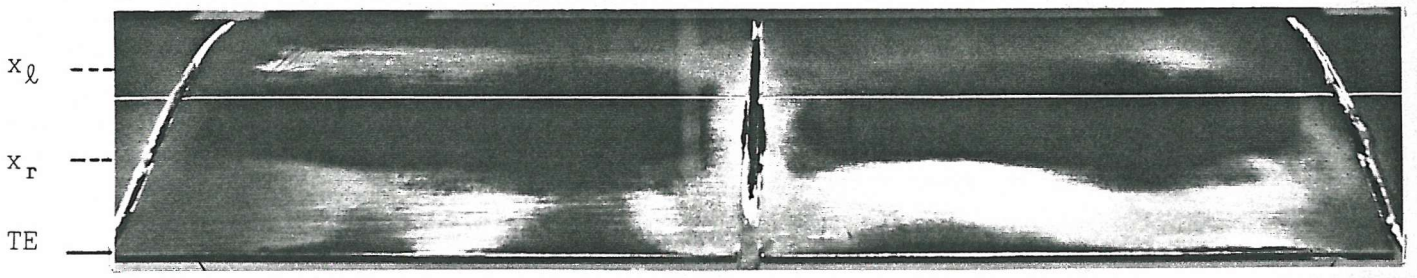

(d) α = 0° upper surface Re = 1.5 x 10^5

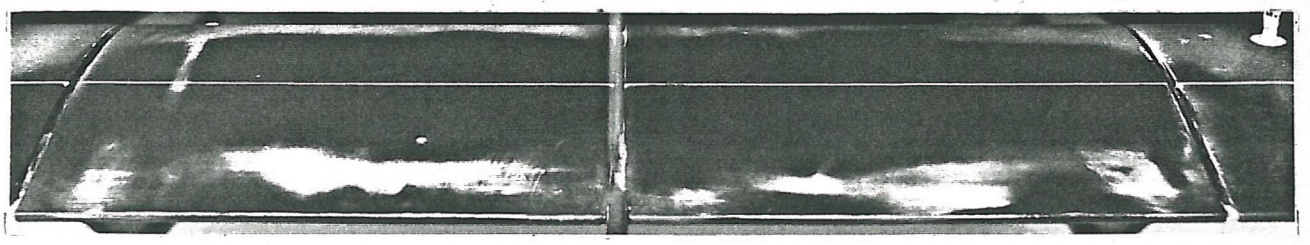

(e) α = 0° under surface Re = 1.5 x 10^5

Fig. 16 Flow visualization results at Re = 2 x 10^5 and 1.5 x 10^5

Fig. 17 Section WF5T tested between end plates at Re = 2.5 x 10^5

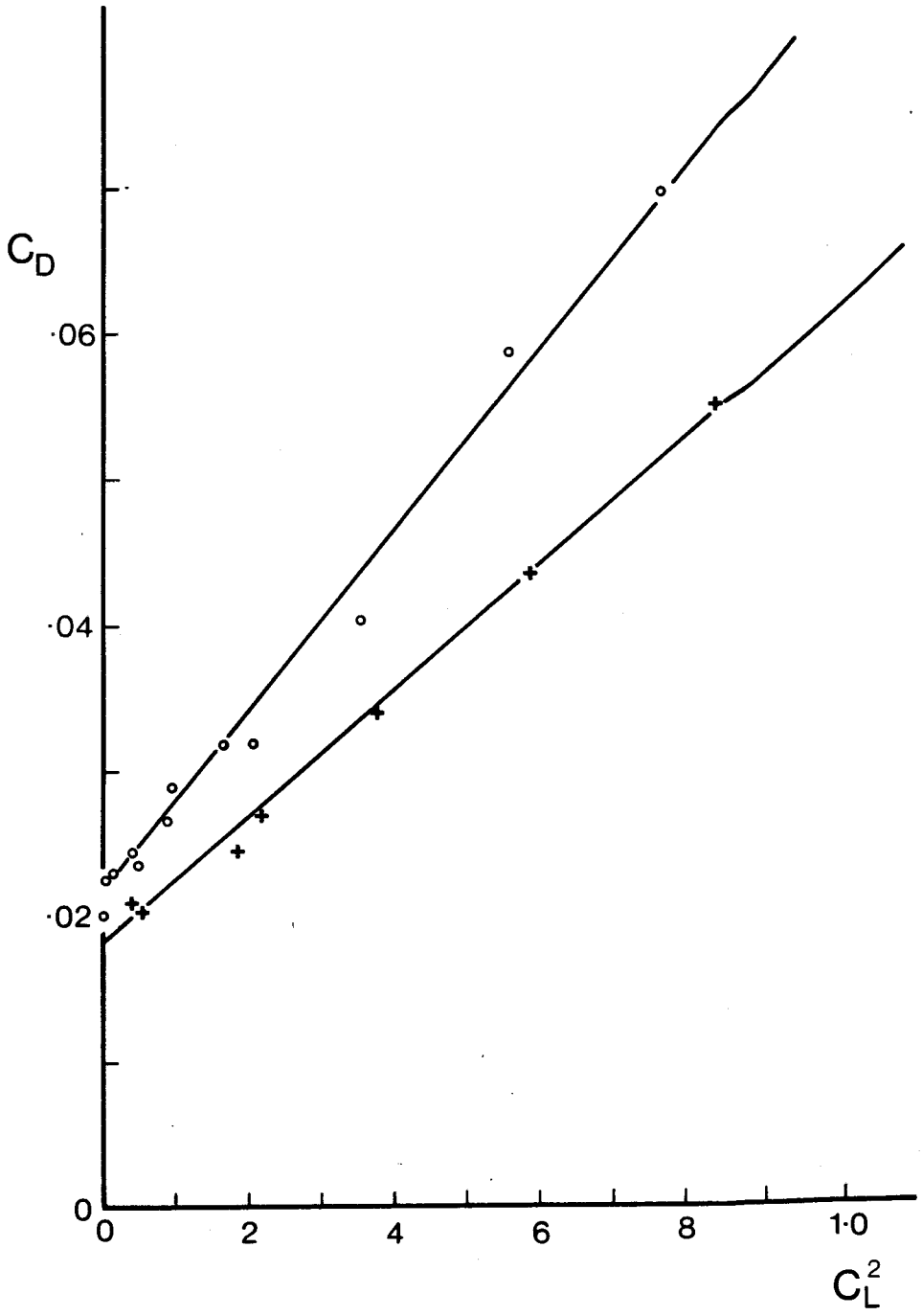

+ 2D fairing section $C_D \sim .0180 + .0433\ C_L^2$

o 3D fairing section $C_D \sim .0215 + .0625\ C_L^2$

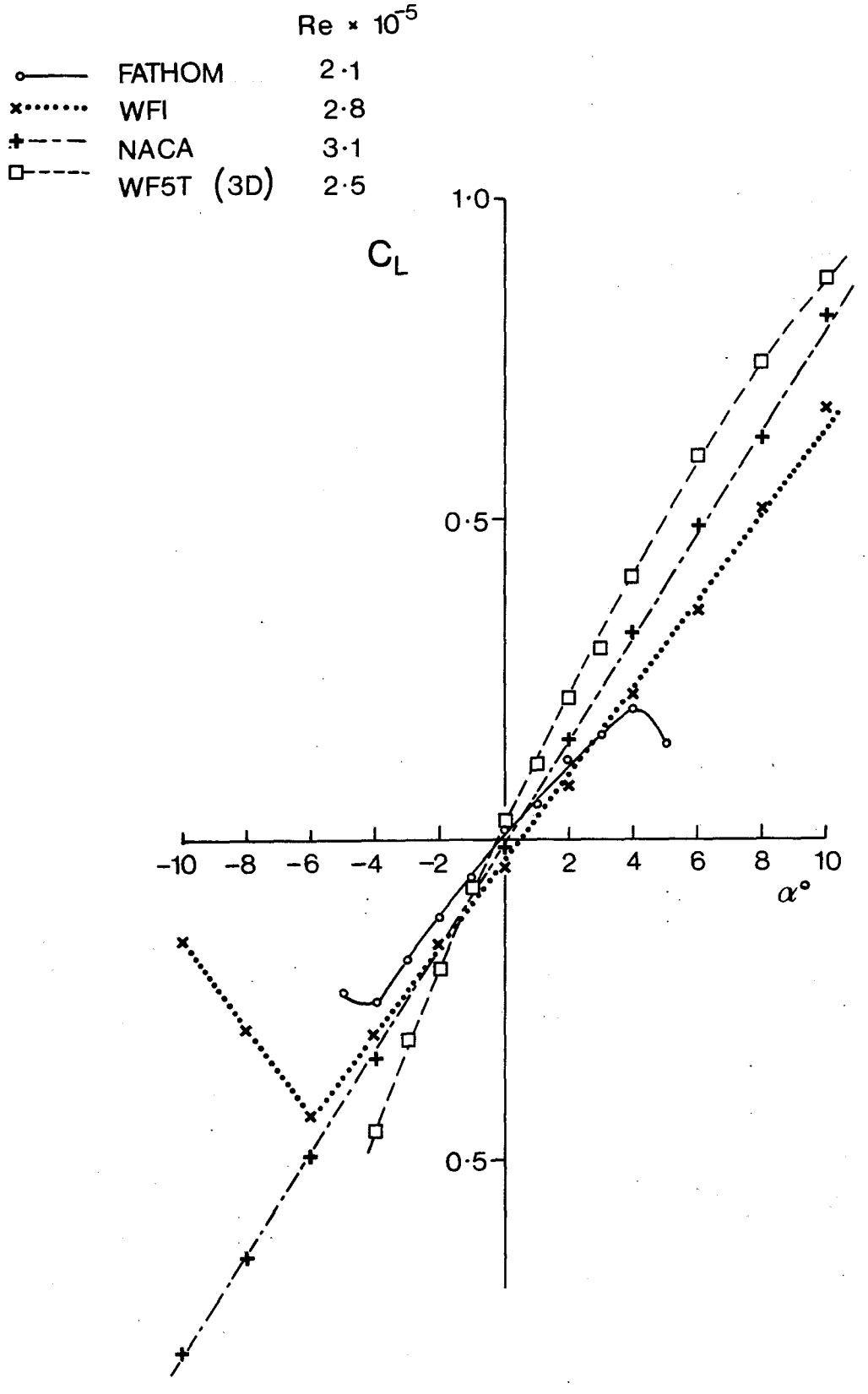

Fig. 18a Comparison of the wind tunnel data obtained for sections WF1, NACA 0021, and WF5T (3D model) with the FATHOM fairing results of Henderson (1978)

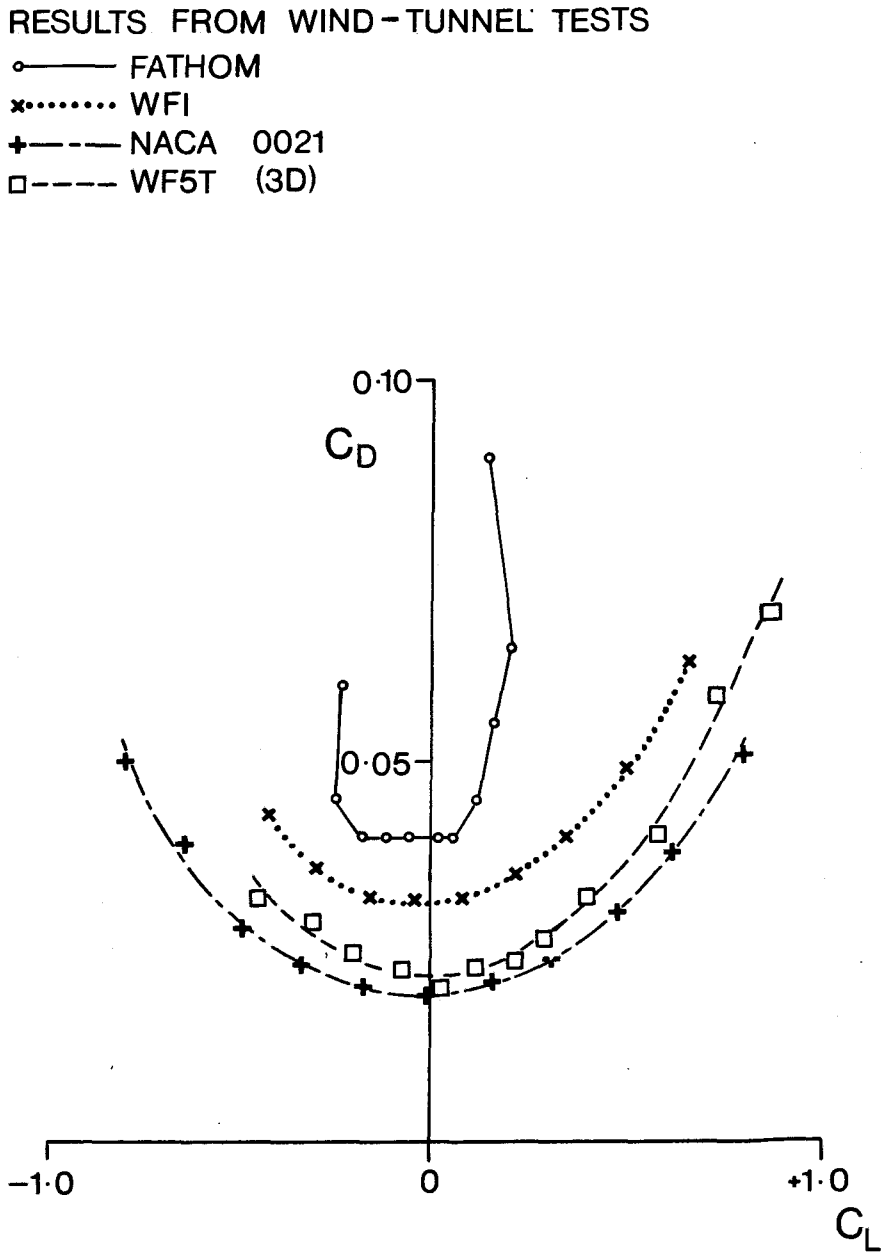

Fig. 18b for caption see fig. 18a

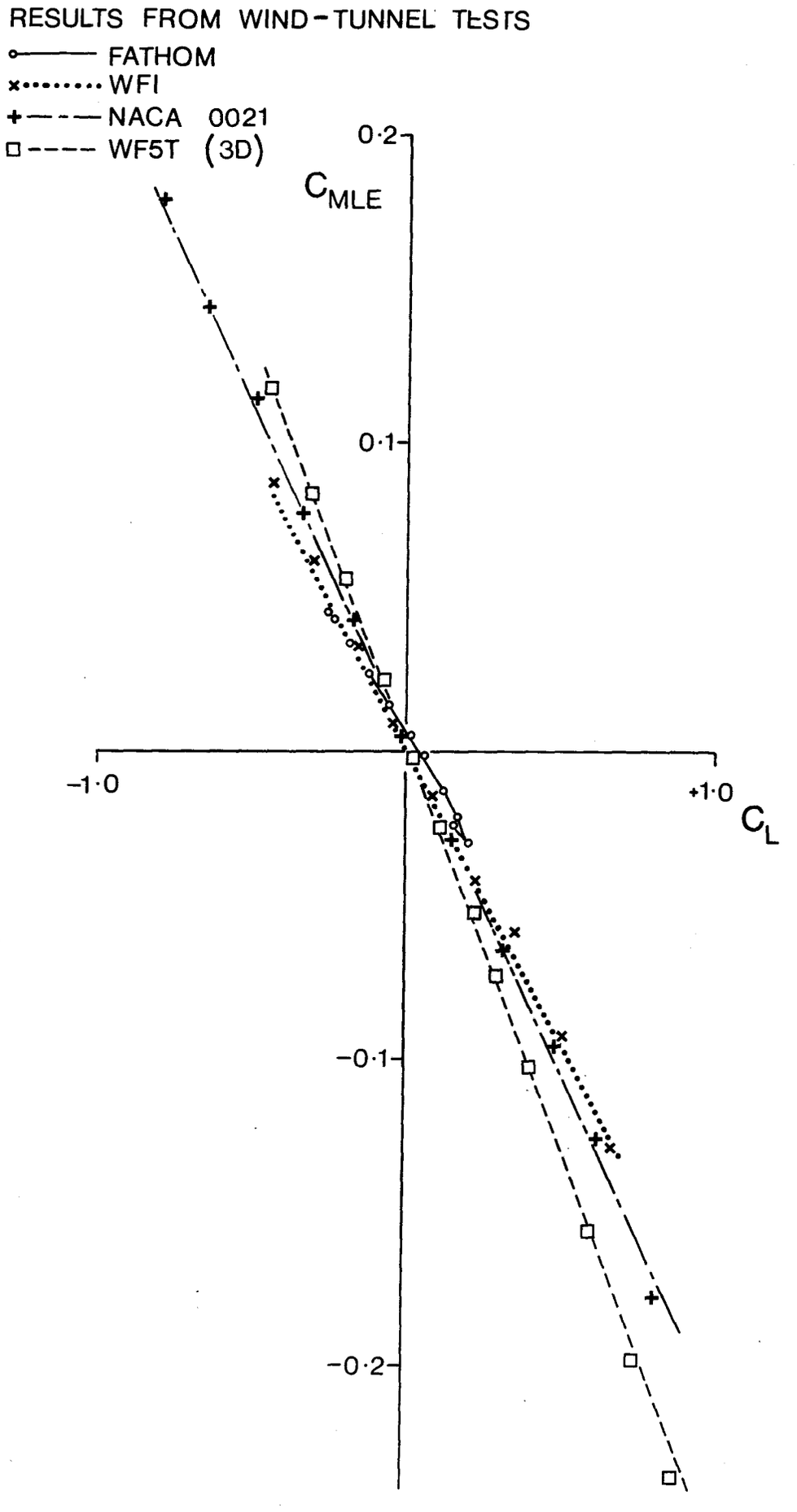

Fig. 18c for caption see fig. 18a

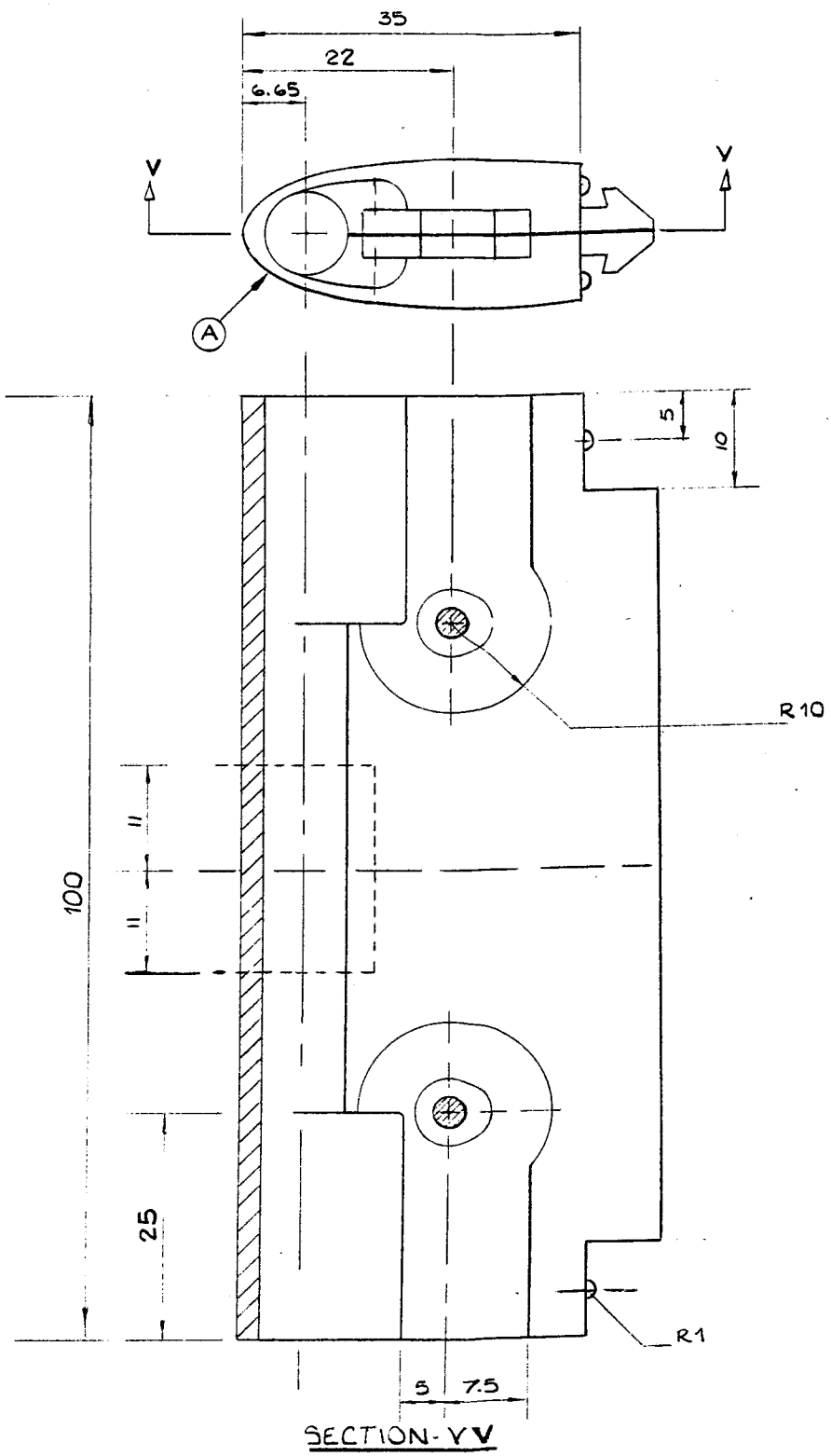

Fig. 19a Drawing of the nose section of a WF5T fairing segment. Dimensions in millimetres. Co-ordinates for curve (A) are given in fig. 20.

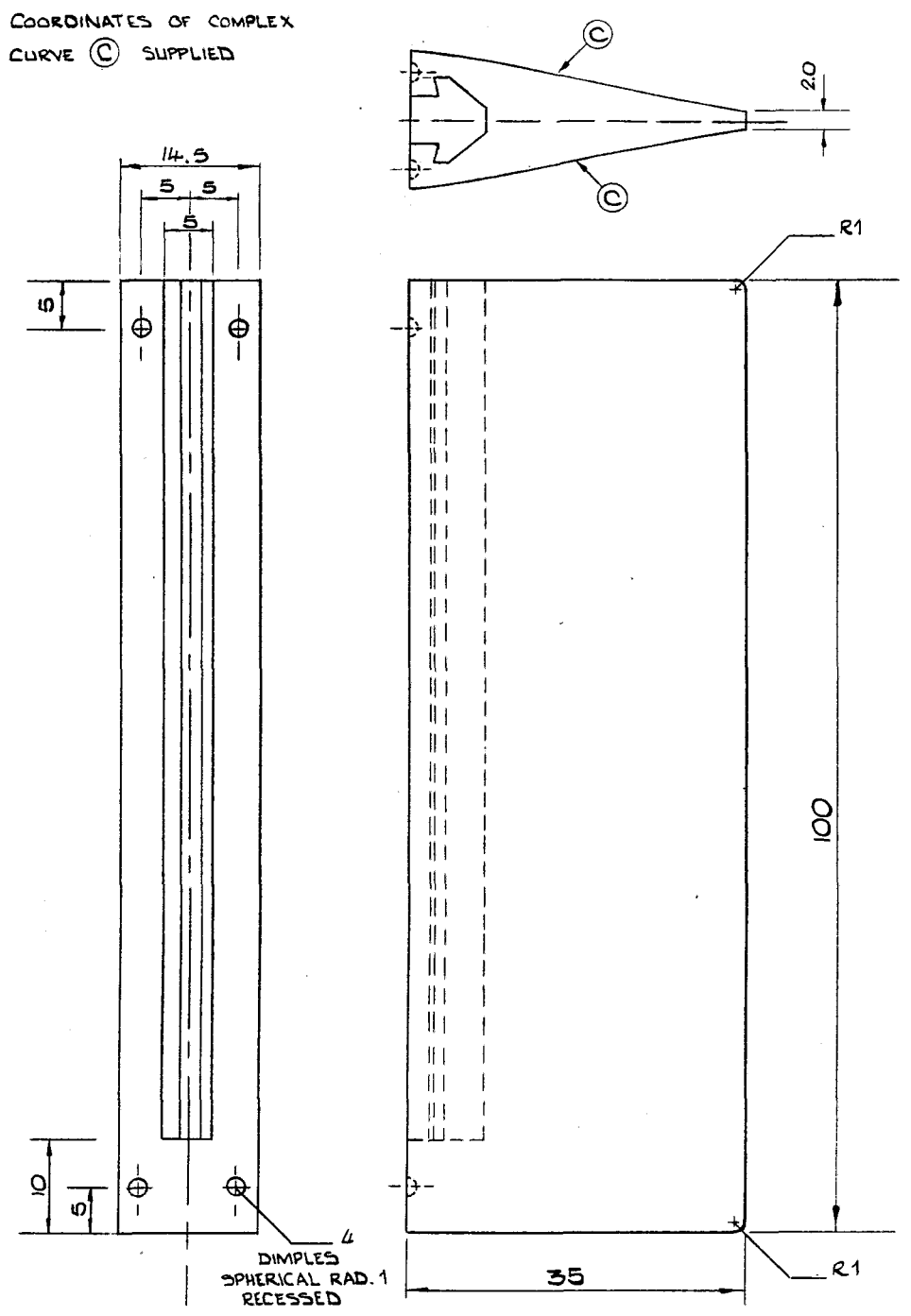

Fig. 19b Drawing of the tail section of a WF5T fairing segment. Dimensions in millimetres. Co-ordinates for curve (C) are given in fig. 20.

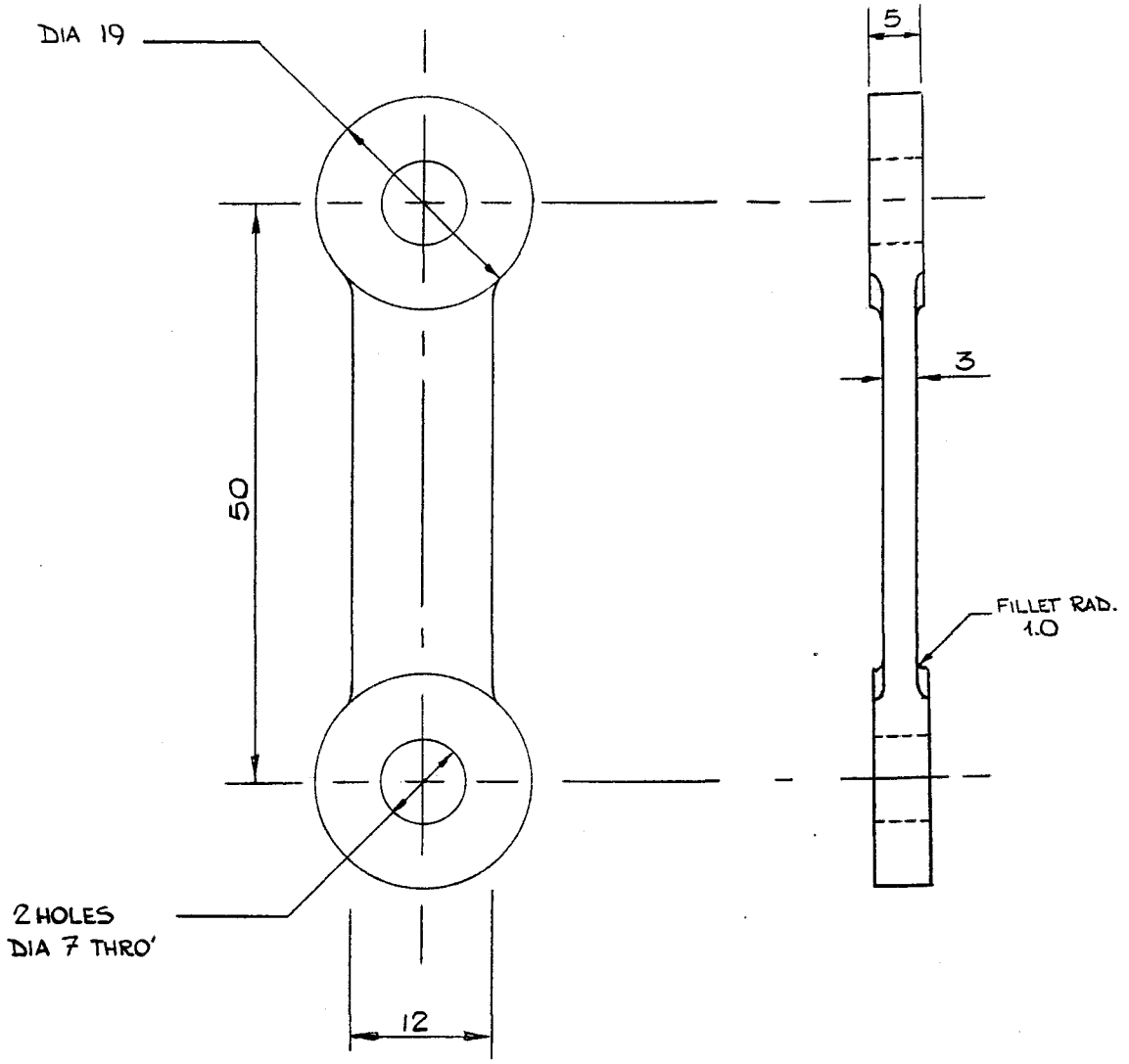

Fig. 19c Drawing of the elastic link joining neighbouring fairing segments. Dimensions in millimetres.

Fig. 20 Full scale surface coordinates for the complex curves (A) and (C) shown in fig. 19

	WEST NOSE	
	X(mm)	Y(mm)
1	0.00	0.00
2	0.19	0.81
3	0.76	2.04
4	1.71	3.14
5	3.03	4.17
6	4.69	5.06
7	6.68	5.83
8	8.99	6.49
9	11.53	7.01
10	14.43	7.42
11	17.50	7.69
12	20.76	7.84
13	24.18	7.86
14	27.72	7.77
15	31.34	7.56
16	35.00	7.25

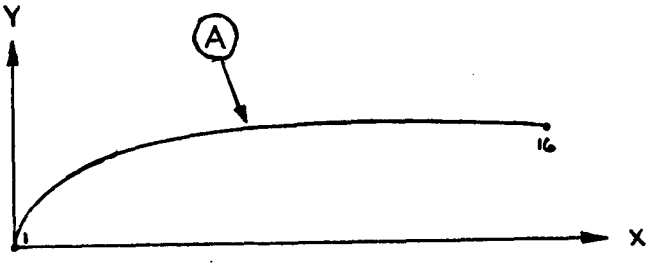

	WEST TAIL	
	X(mm)	Y(mm)
1	0.00	7.25
2	3.66	6.83
3	7.28	6.29
4	10.82	5.61
5	14.24	4.89
6	17.50	4.20
7	20.57	3.56
8	23.42	2.99
9	26.01	2.50
10	28.32	2.09
11	30.31	1.74
12	31.97	1.47
13	33.29	1.27
14	34.24	1.13
15	34.81	1.05
16	35.00	1.01

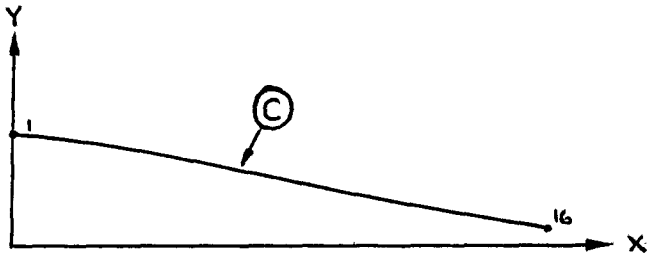

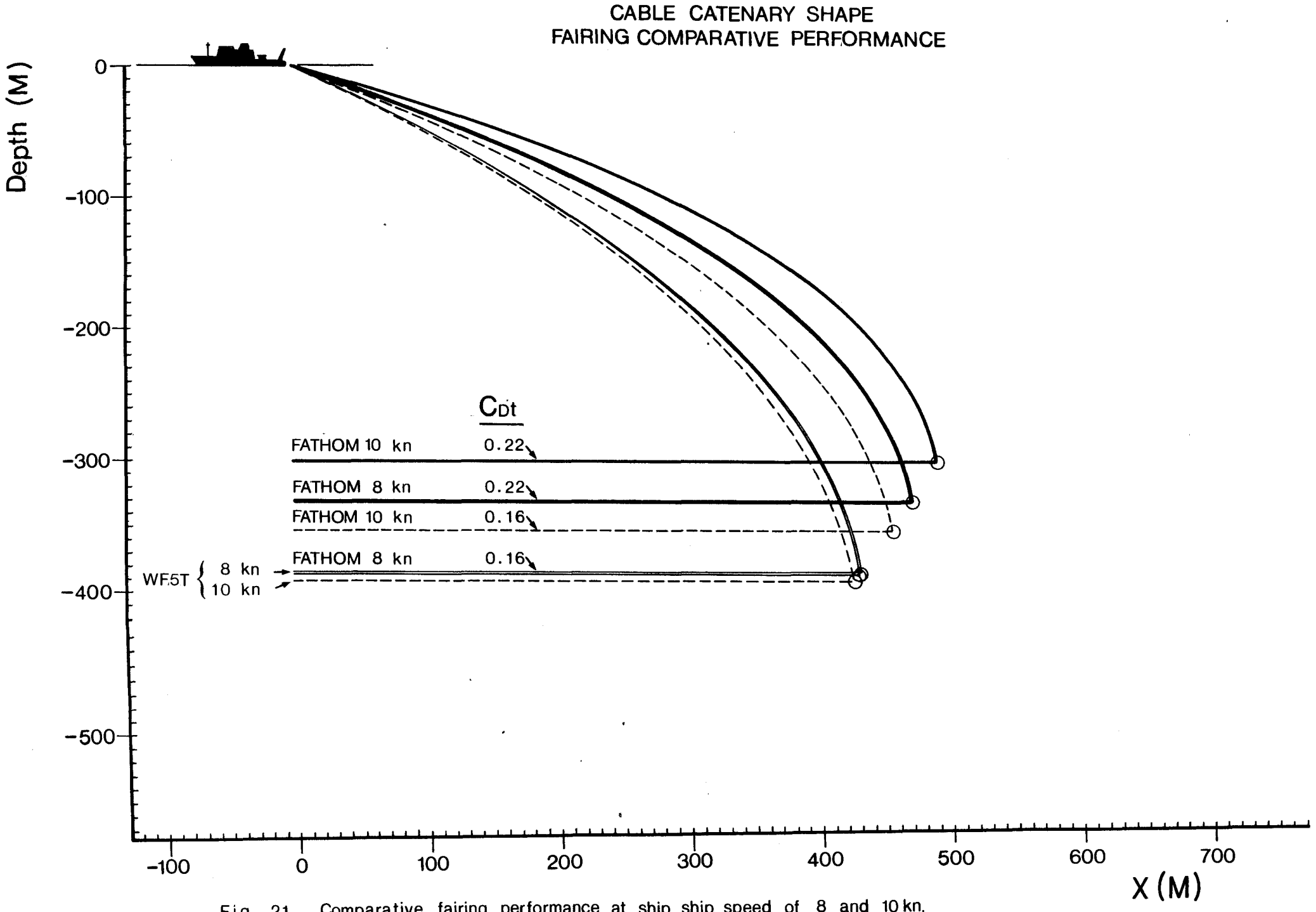

Fig. 21 Comparative fairing performance at ship ship speed of 8 and 10 kn.

Appendix

Wind tunnel corrections

The model was mounted inverted in the tunnel so that, as viewed, positive incidence was nose down as shown below. C_L', C_D', C_M' were measured at the pivot point A.

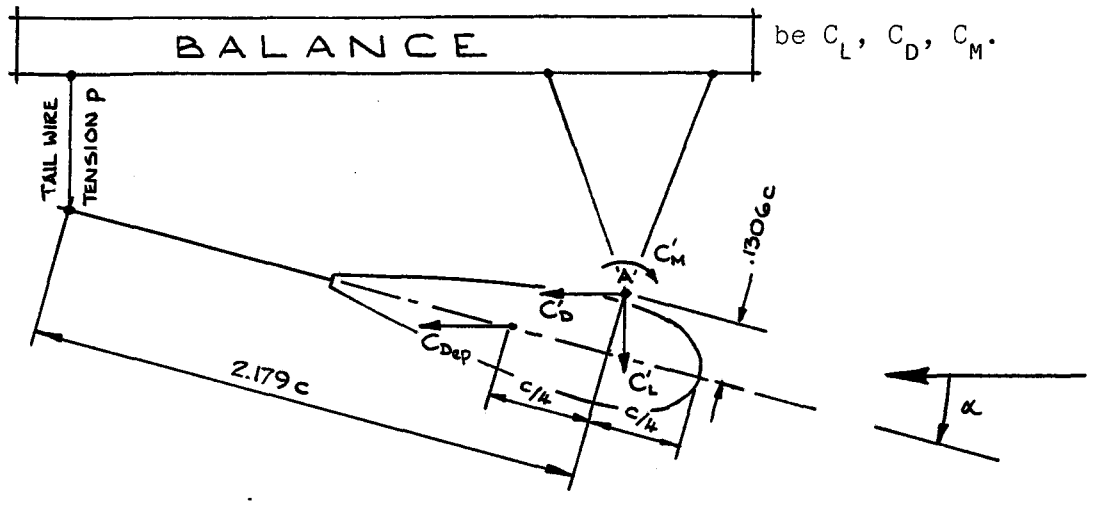

Let the corrected coefficients be C_L, C_D, C_M.

1) Moment correction

Moments are positive nose up therefore a down load on the tail-wire (nett p +ive) represents a nose down moment.

$$\therefore \quad C_M' = - \frac{p}{\frac{1}{2}\rho V^2 Sc} \quad (2.179 \cos \alpha + 0.1306 \sin \alpha)c$$

The moment due to the wires was approximated by

$$C_{MW} = - 0.00068 + 0.00011\alpha \qquad \text{where } \alpha \text{ is in degrees.}$$

If the moments are to be taken about the quarter chord point then allowing for the wire moment and the end plate drag moment

$$C_{Mc/4} = C_M' + C_{MW} + 0.25\, C_{Dep} \sin \alpha + 0.1306\, (C_D' \cos \alpha - C_L' \sin \alpha)$$

or alternatively about the leading edge

$$C_{MLE} = C_{Mc/4} - 0.25\, (C_L \cos \alpha + C_D \sin \alpha)$$

Appendix - page 2

2) Drag corrections

Drag due to wires $C_{DW} = 0.0155$

Drag due to end-plates $C_{Dep} = 0.0222$

Tunnel constraint drag $C_{Dtc} = C_L \sin(\Delta\alpha_{tc})$

where the change in incidence due to tunnel constraint $\Delta\alpha_{tc} = 0.918\, C_L$

$$C_D = C_D' - C_{DW} - C_{Dep} + C_{Dtc}$$

3) Incidence correction

For free flow $\alpha_{eff} = \alpha + \Delta\alpha_{tc}$

$$C_L(\alpha_{eff}) = C_L'(\alpha)$$

4) Blockage corrections

Correction factor to coefficients - with end plates = 0.994

without end plates = 0.996